Available online at https://link.springer.com/journal/42241
http://www.jhydrodynamics.com
Journal of Hydrodynamics, 2023, 35(5): 832-857
https://doi.org/10.1007/s42241-023-0071-6

Recent progress on the jetting of single deformed cavitation bubbles near boundaries

Jing-zhu Wang[1, 2, 6], Guang-hang Wang[1, 3], Qing-yun Zeng[4, 5*], Yi-wei Wang[1, 2, 3*]
1. *Key Laboratory for Mechanics in Fluid Solid Coupling Systems, Institute of Mechanics, Chinese Academy of Sciences, Beijing 100190, China*
2. *School of Engineering Science, University of the Chinese Academy of Sciences, Beijing 100049, China*
3. *School of Future Technology, University of the Chinese Academy of Sciences, Beijing 100049, China*
4. *College of Shipbuilding Engineering, Harbin Engineering University, Harbin 150001, China*
5. *Nanhai Institute of Harbin Engineering University, Sanya 572024, China*
6. *Guangdong Aerospace Research Academy, Guangzhou 511458, China*

(Received April 24, 2023, Revised August 21, 2023, Accepted August 22, 2023, Published online December 12, 2023)

Abstract: Cavitation occurs widely in nature and engineering and is a complex problem with multiscale features in both time and space due to its associating violent oscillations. To understand the important but complicated phenomena and fluid mechanics behind cavitation, a great deal of effort has been invested in investigating the collapse of a single bubble near different boundaries. This review aims to cover recent developments in the collapse of single bubbles in the vicinity of complex boundaries, including single boundaries and two parallel boundaries, and open questions for future research are discussed. Microjets are the most prominent features of the non-spherical collapse of cavitation bubbles near boundaries and are directed toward rigid walls and away from free surfaces. Such a bubble generally splits, resulting in the formation of two axial jets directed opposite to each other under the constraints of an elastic boundary or two parallel boundaries. The liquid jet penetrates the bubble, impacts the boundary, and exerts a great deal of stress on any nearby boundary. This phenomenon can cause damage, such as the erosion of blades in hydraulic machinery, the rupture of human blood vessels, and underwater explosions, but can also be exploited for applications, such as needle-free injection, drug and gene delivery, surface cleaning, and printing. Many fascinating developments related to these topics are presented and summarized in this review. Finally, three directions are proposed that seem particularly fruitful for future research on the interaction of cavitation bubbles and boundaries.

Key words: Jetting cavitation bubble, near complex boundaries, bubble-based technique and their applications

0. Introduction

Cavitation is a fascinating hydrodynamic phenomenon that occurs ubiquitously in nature and engineering applications. It refers to the formation, growth, and collapse of cavitation bubbles due to the breakdown of liquid under very low local pressures in high-speed flows. Through violent oscillations in both shape and volume, cavitation bubbles can produce significant mechanical and thermal effects in the liquid medium and on the surrounding boundaries. These remarkable effects and inherent complex dynamics have made cavitation a topic of long-standing interest in fields such as hydraulic machinery and biomedical engineering.

The study of cavitation began with Reynolds and Parsons, who examined the failed trial of a British warship in 1885. They suggested that an implosion of water vapor bubbles damaged the propeller blade and named this phenomenon “cavitation”. The destructive effects of cavitation can cause damage and breakdowns in numerous other types of hydraulic machinery, including hydraulic turbines, pumps, and artificial heart valves. The associated flows typically cavitate within their low-pressure zones, such as regions of flow separation and vortex cores. In nature, the destructive potential of cavitation is used as an effective tool by peacock mantis shrimps to hunt their prey. Furthermore, cavitation also occurs in liquid-propelled rocket engines, lubricated bearings trees,

Project supported by the National Natural Science Foundation of China (Grant Nos. 12122214, 12272382, 12293000, 12293003 and 12293004).
Biography: Jing-zhu Wang (1989-), Female, Ph. D., Associate Professor, E-mail: wangjingzhu@imech.ac.cn
Corresponding author: Qing-yun Zeng, Yi-wei Wang, E-mails: qyzeng@hrbeu.edu.cn, wangyw@imech.ac.cn

inkjet printing, and microfluidic pumps. Biomedical fields also benefit from the remarkable properties of cavitation for destroying kidney stones during lithotripsy, emulsifying the natural optical lens during cataract surgery, delivering drugs and targeting cells in a highly controllable way, intraocular surgery, and needle-free drug injection.

Cavitation is a complex problem with multiscale features in both time and space resulting from violent oscillations. Cavitation bubbles are seldom spherical, as they form next to boundaries. Instead, they deform and produce jets when interacting with nearby boundaries. These processes also generate vortices, shock-waves, toroidal bubbles, and the breakup of surfaces at various stages of the bubble dynamics. To understand the important but complicated phenomena and fluid mechanics behind these processes, much effort has been invested in investigating the collapse of a single bubble near different boundaries. The literature related to bubble dynamics and cavitation has been summarized by several researchers since 1977[1-6]. Cavitation bubbles near boundaries were reviewed first by Blake and Gibson in 1987 in the Annual Review of Fluid Mechanics[2]. At that time, although experimental observations with high-speed cameras led to developments in understanding the collapse of a cavitation bubble, most of these results were restricted to a sequential picture of the bubble shape, leading to estimates of particle velocities on the bubble surface. Few attempts were made to measure pressures on the boundaries. Thirty years later, fantastic progress has been made in theoretical modeling, experimental observations, and numerical simulations. Prosperetti[4] summarized the fundamental physics of vapor bubbles in liquids, and in particular, the essential differences from bubbles mostly containing a permanent gas. The article showed that experiments on vapor bubbles are of particular value in shedding light on the detailed physics of phase changes, some aspects of which are still very poorly understood. Dollet et al.[6] reviewed recent developments in bubble dynamics in soft and biological matter for different confinement conditions. In contrast with articles published in the Annual Review of Fluid Mechanics, this review focuses on recent developments and new phenomena related to the physical mechanisms and engineering applications of the collapses of single cavitation bubbles near single and parallel boundaries.

1. Bubble collapse near single boundaries

1.1 *Rigid walls*

The non-spherical collapse of a cavitation bubble near a rigid wall is a classic topic in bubble dynamics and critical to understanding the mechanism of erosion by hydrodynamic cavitation. During non-spherical collapse, a cavitation bubble creates a high-speed re-entrant jet directed toward the rigid surface. Upon impact, the water hammer pressure produced is considered sufficiently high to erode the wall surface. The liquid jet then spreads along the rigid surface with high shear rates after the impingement, which is beneficially exploited in fields such as ultrasonic cleaning and ultrasonic mixing. The details of the bubble dynamics and jet formation near boundaries strongly depend on the stand-off distance $\gamma = d / R_{\max}$ which is defined as the distance of the initial location of the bubble center from the boundary d scaled by the maximum bubble radius $R_{\max}$.

1.1.1 Cavitation-induced microjets

Kornfeld and Suvorov[7] were the first to suggest that a bubble might collapse asymmetrically and produce a re-entrant jet pointing toward a rigid wall due to the existence of a pressure gradient[8]. Since then, the jetting dynamics of a cavitation bubble near a rigid wall has been widely studied via experiments, numerical simulations, and theoretical modeling[9-14]. Many studies have suggested that the re-entrant liquid jet reaches a velocity of the order of 100 m/s, and a diameter approximately 10%-30% of the maximum bubble diameter, i.e., a cavitation bubble of 2 mm diameter produces a jet that is approximately 200 μm-600 μm wide at $\gamma > 0.3$. Overall, the jet velocity increases with γ for $\gamma > 0.3$.

Recently, the formation and characteristics of jets have been investigated for bubble collapses extremely close to a rigid wall. Lechner et al.[15] reported the generation of very fast and thin jets when $\gamma < 0.2$ using axisymmetric volume of fluid (VOF) simulations. Such jets were found to propagate at supersonic speed inside the bubble and even reached ~1 300 m/s for $\gamma = 0.1$, which is an order of magnitude faster than the regular jet mentioned above. This type of jet is called a needle jet in the study by Reuter and Ohl, who studied its dynamics using ultra-high-speed imaging at five million frames per second with femtosecond illuminations[16]. A special observation is shown in Figs. 1(a_1), 1(a_2), with a kink appearing at the bubble surface at the late stage of the collapse, which is the result of a boundary-parallel cylindrical flow that converges on the axis of symmetry. The kink then hits the axis of symmetry and creates a high pressure at the stagnation point, which instantaneously accelerates the liquid downwards, leading to the formation of the needle jet. This jet formation mechanism was also confirmed numerically by Lechner et al.[17], as shown in Fig. 1(b). What makes the needle jet distinct from a regular jet is the presence of a

cylindrical flow converging on the axis of symmetry before the bubble's top surface develops into a jet. Such a process magnifies the driven pressure to be a hundredfold larger than that of a regular jet, and therefore the jet is accelerated to 10 times the speed. A similar phenomenon has also been observed in other axisymmetric convergent flows, such as the so-called Worthington jet[18-20]. The stand-off regime of the needle jet is rather narrow, as identified by Reuter et al. (Fig. 1(c)). However, the thin jet detail inside the bubble has not been captured due to the inherent difficulty of using a visible light source for illumination in a shadowgraph. However, the details of regular jets and toroidal bubbles can be clearly visualized using a phase-contrast imaging method with an X-ray as a light source[21], which might be one solution for revealing the needle jet experimentally.

The velocity of a microjet is an important parameter in evaluating the strength of the impact, whether disruptive or beneficial. For example, the impingement of a liquid jet on a rigid boundary creates a water hammer pressure whose peak value is approximately

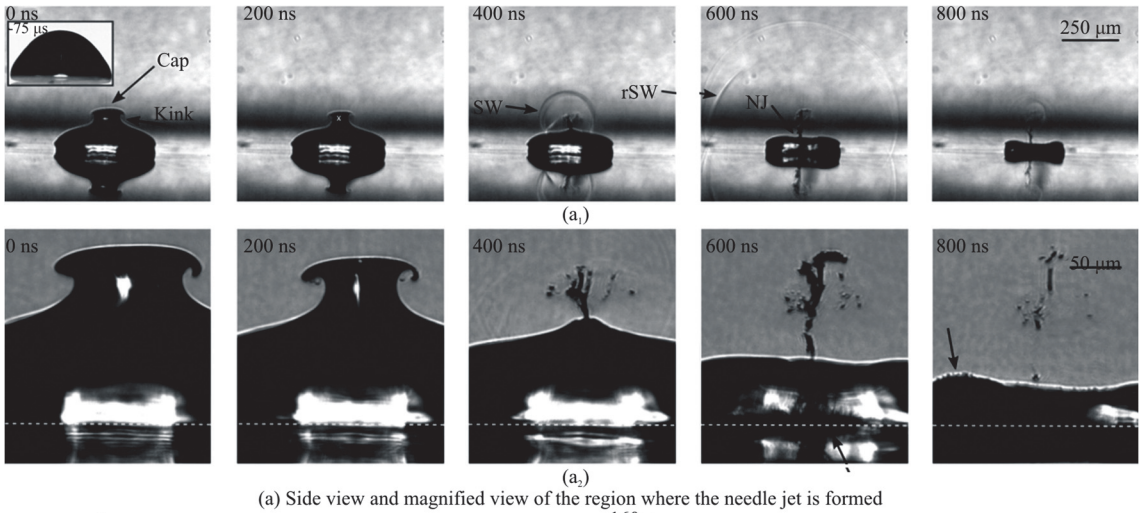

(a) Side view and magnified view of the region where the needle jet is formed

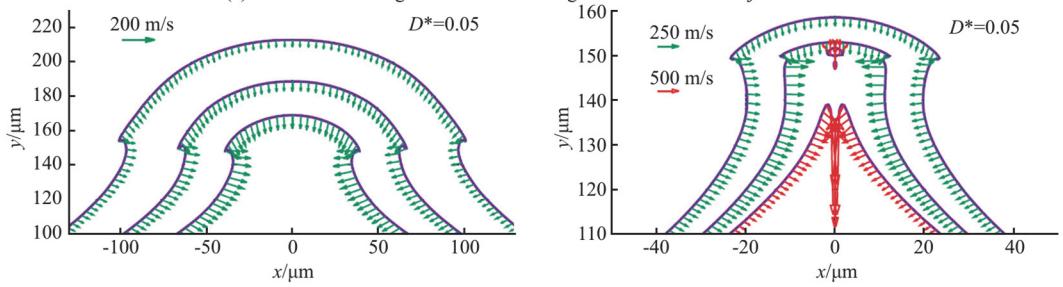

(b) Velocity fields obtained from a numerical simulation

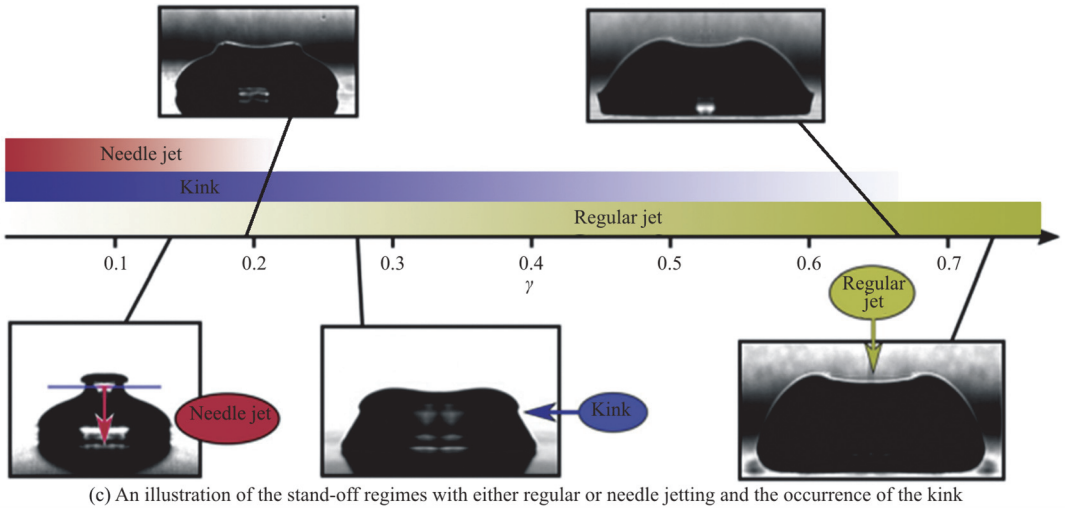

(c) An illustration of the stand-off regimes with either regular or needle jetting and the occurrence of the kink

Fig. 1 (Color online) The formation and development of the needle jet. In (c), three regimes are classified: (1) The formation of the needle jet ($\gamma < 0.17$), (2) The formation of the cylindrically convergent flow, resulting in a circumferential kink ($\gamma < 0.68$) and (3) The formation of the regular jet ($\gamma > 0.17$) [16, 30]

linearly dependent on the impact velocity. As the microjet velocity is of the order of 80 m/s, the resulting water hammer pressure can reach 100 MPa, which is higher than the yield strength of most materials. Until now, numerous numerical and experimental studies have attributed the cavitation erosion of material surfaces to the impact of microjets[22-24]. However, the microjet velocity is found to be a complex function of the stand-off distance g, as shown in Fig. 2. A separation in jet regimes around $\gamma = 0.2$ is created by different sources of the driven pressure acting on the top surface during jet formation. For the regular jet, the driven pressure is the pressure that builds up near the bubble's top surface as the bubble shrinks. Meanwhile, for a needle jet, this driven pressure comes from the stagnation pressure when the annular flow hits the axis, which is one order higher than that of a regular jet. The microjet velocity increases as the bubble moves away from the rigid boundary when $\gamma > 0.2$. However, the strength of the jet acting on the boundary might not increase. This is because a liquid film exits between the rigid boundary and the bubble's lower surface[25]. The re-entrant jet has to travel in water for a certain distance before reaching the wall after piercing the bubble's lower surface. This results in a significant loss of energy that attenuates the jet speed and subsequent impact pressure. In contrast, for small stand-off distances, the microjet hits the wall almost simultaneously and therefore has a higher impact pressure. However, the role of microjets has remained inconclusive since in some works, under some circumstances, no damage from the jet was reported, or the surface damage as a function of γ was not consistent[26-29].

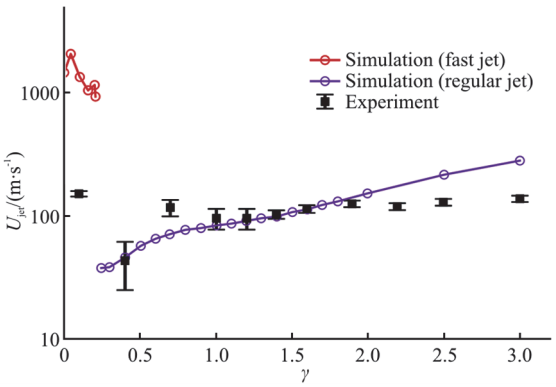

Fig. 2 (Color online) The jet velocity U_{jet} versus the stand-off distance γ. The filled squares are experimental data from Phillip and Lauterborn[9], while the open circles are simulation results from Lechner et al.[30]. The simulation indicates a separation in jet regimes around $\gamma = 0.2$, below which supersonic fast and thin jets (also called needle jets by Reuter and Ohl[16]) occur

1.1.2 Shockwaves

Multiple shock waves are induced at various stages. For instance, during the initial expansion, a high-speed microjet pierces the lower bubble surface, and the bubble reaches its minimum volume and subsequently collapses after a rebound. The timing, duration, and strength of the shock waves have been analyzed in experiments and simulations. Yet an understanding of the contribution of each shock emission mechanism behind bubble deformation near a rigid wall is still lacking due to the insufficient bandwidth of the sensor and frame rates in experiments and limitations in multiscale modeling. The fast-rising pressure behind the shock front can reach GPa values within a few nanoseconds and is applied in engineering applications such as shock wave lithotripsy cancer therapy, and sterilization.

Blake et al.[31] captured and described the origin of multiple shock waves radiated as a cavitation bubble approach and reaches its minimum volume using a high-speed camera with a frame rate of 2.0×10^7 per second. Although limited to eight frames captured in one experiment, their observations are valuable for achieving a better understanding of the recorded acoustic traces. Compared with spherical collapse, the compression of the bubble content is less violent, and sound emissions are diminished as the jet penetrates through the bubble, leading to a toroidal bubble before it reaches its minimum volume[32]. Moreover, upon impact, a splash occurs and ejects liquid into the toroidal bubble. The distorted and collapsing toroidal bubble then generates a vortex ring when the jet spreads. Under these circumstances, energy is transferred to the rotation of the toroidal bubble and the jet, and as a result, the bubble is compressed less. Recently, more experimental studies have been carried out to precisely measure the shockwave. Supponen et al.[33] estimated the strengths and timings of the distinct shock waves produced by the collapse of bubbles with geometries varying from highly spherical to strongly deformed by a nearby free surface. Gonzalez-Avila et al.[34] systematically analyzed the acoustic transient for $0.4 \le \gamma \le 5.2$. They measured a peak pressure of up to 10^5 kPa generated during the collapse of a bubble, which lasted for several tens of nanoseconds. These shock waves generated by the collapse of the bubble were shown to propagate radially outward along the rigid wall. Such emitted shock waves were also identified as the main sources of cavitation erosion[35]. However, large temperatures are expected to develop as the bubble proceeds toward its minimum volume[36-39]. This makes acoustic pressure evaluation exceedingly demanding. The prediction of the damage potential of shock waves emitted by non-spherically collapsing bubbles is still an open problem.

1.1.3 Vortex and wall shear flow

After jet impact, two flow patterns are found depending on the stand-off distance between the bubble and the wall: (1) A free vortex that translates into the bulk liquid away from the rigid wall. (2) A wall vortex that moves along the wall and spreads radially over the wall.

Brujan et al.[40] conducted a numerical simulation to investigate the velocity and pressure fields in the liquid surrounding a bubble. They found that a vortex ring was formed after the jet impacted the boundary and then spread along the boundary. Reuter et al.[41] investigated the flow fields of bubble collapse using a hybrid particle image velocimetry/particle tracking velocimetry (PIV/PTV) technique and summarized the vortex behavior as a function of γ: A free vortex for $0.5 \le \gamma \le 1.3$ and a wall vortex for $\gamma \ge 1.36$. The radius of the circular region of a high wall shear from the stretching vortex can exceed the maximum radius of the vortex-generating bubble. The generation of a wall vortex and free vortex was also identified when a laser-induced bubble oscillated near the sand bed in a study by Sieber et al.[42]. This study showed that the subsequent formation and development of vortex flows are determined mainly by the way that bubbles collapse. Saini et al.[43] conducted a direct numerical simulation of the formation of a vortex ring after the collapse of a bubble. Figure 3 shows the velocity fields in two representative cases: A free vortex and a wall vortex. Their results revealed that during the collapse, an annular jet parallel to the wall is formed, resulting in an upward flow that generates a free vortex. Huang et al.[44] carried out a numerical simulation to analyze the effects of wall wettability on vortex flows induced by collapses of cavitation bubble near a rigid wall (see Fig. 4). The wall wettability was modeled by the contact angle and slip velocity.

Cavitation bubbles are known to induce a strong shear flow on the rigid surface to remove attached dirt particles and thus clean the surface. Ohl et al.[45] captured the motion of fluorescent particles on surfaces with streak images to resolve the tangential flow from a laser-induced bubble at four representative stages. They found that the jet impact process promotes the most prominent wall shear flow rather than the other three stages, i.e., bubble expansion, bubble collapse, and re-expansion. They also indicated that the highest shear stress from oscillating cavitation was applied on the wall, thus cleaning it during a short time interval. Later, Dijkink and Ohl[46] directly measured the shear stress τ of a near-boundary flow with a hot-film anemometer inserted on a rigid surface. The stress recording showed an interesting trace and was explained with images of bubbles from high-speed photography. The trace is shown in Fig. 5(a). The stress increases rapidly to its peak value of 3.5 kPa right after the jet impact. During the decay, the shear stress rises again to a second peak but with a much lower amplitude due to the re-expansion of the bubble. Soon afterward, however, the shear stress decreases

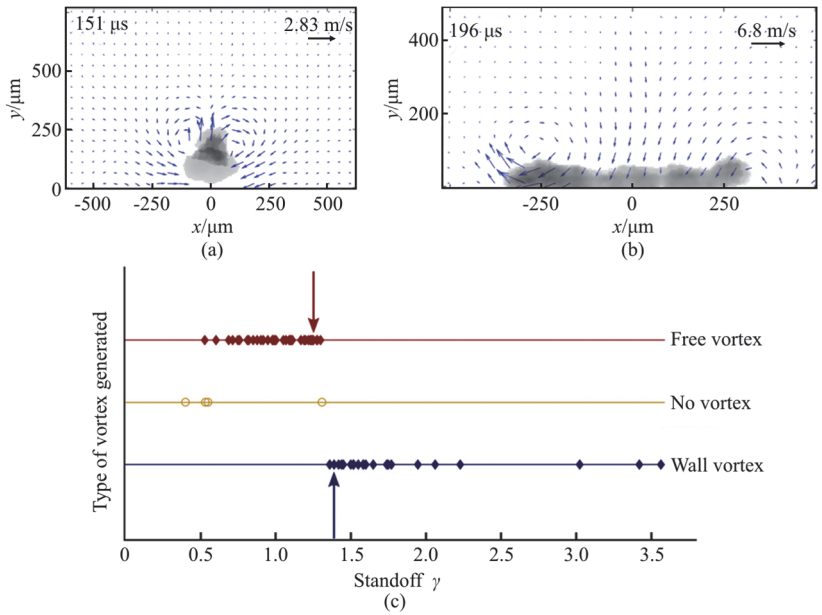

Fig. 3 (Color online) Patterns of vortex flows induced by the jetting of a cavitation bubble near a rigid wall: (a) PIV measurement of a cavitation bubble with $\gamma = 1.21$, collapse time $T_L = 68\ \mu s$, maximum bubble radius $R_{max} = 325\ \mu m$, with the free vortex seen after the first collapse of the bubble, (b) PIV measurement of a cavitation bubble with $\gamma = 1.75$, $T_L = 80\ \mu s$, $R_{max} = 420\ \mu m$, with a wall vortex seen during the first collapse of the bubble and (c) Distributions of the vortex as a function of the stand-off distance γ [41]

with a small decaying speed as the vortex ring is involved. Yet, due to the low temporal bandwidth, the amplitudes reported are lower bound. Reuter and Mettin[47] developed another electrochemical fast sampling technique to measure the wall shear stress. Their device allowed scanning of the substrate to obtain a spatial distribution of the wall shear stress by repeating the same experiment many times. The wall shear rate was obtained by solving a convection-diffusion equation with the measured microelectrode signal as input. They recorded a maximum stress value of 6.2 kPa. Yet, apart from the inherent low bandwidth, both measurements ignored the particular boundary layer structure and assumed a laminar constant shear due to experimental challenges associated with resolving a multiscale fast flow. Using a sufficiently fine grid and a robust compressible VoF solver, Zeng et al. simulated the dynamics of a laser-induced cavitation bubble with a wall distance $\gamma \approx 1.0$ and revealed the complex boundary flow and wall shear stress distribution[48], as shown in Figs. 5(b), 5(c). Their study provided a detailed overview of the spatiotemporal dynamics of the wall shear stress by introducing a spatiotemporal map. They found that the stress created by the spreading jet may reach a peak value of 100 kPa, which is one order of magnitude higher than the corresponding experimental measurements. The simulation also identified a thin boundary layer thickness of only 2 μm for a bubble with a maximum radius of 600 μm when the largest shear occurred.

1.1.4 Cavitation erosion

Cavitation erosion can be attributed to multiple mechanisms, including transient shockwaves, impinging liquid jets, and the subsequent collapses of remnant surface-attached bubbles. Many studies have investigated the effects of individual processes through a post-damage analysis of surface damage on metals caused by a series of single subsequent cavitation events. Dular et al.[29] conducted high-speed observations of surface damage caused by the collapse of a single cavitation bubble. They acquired the following main findings: (1) The most pronounced mechanism of surface erosion is the impact of the microjet for a bubble of $\gamma \le 0.2$. (2) when $\gamma \ge 0.5$, the influence of the microjet diminishes and the collapse of the remnant microscopic bubbles in the rebounded cloud (ring) becomes important. (3) When an external shear flow is involved, the main source of the erosion mechanism is still the microjet, but some minor damage can be induced by the secondary (ring) collapse for $0.5 \le \gamma \le 1.4$ as the bubble residuals move closer and even attach to the surface. Recently, more studies have combined state-of-the-art experimental techniques, such as confocal profilometer and scanning electron microscopy, and numerical tools accounting for complicated fluid material interactions to complement the mechanism of cavitation erosion. Sagar and Moctar[49] applied a novel approach to correlate first and second bubble collapses with the corresponding damage patterns on an aluminum surface.

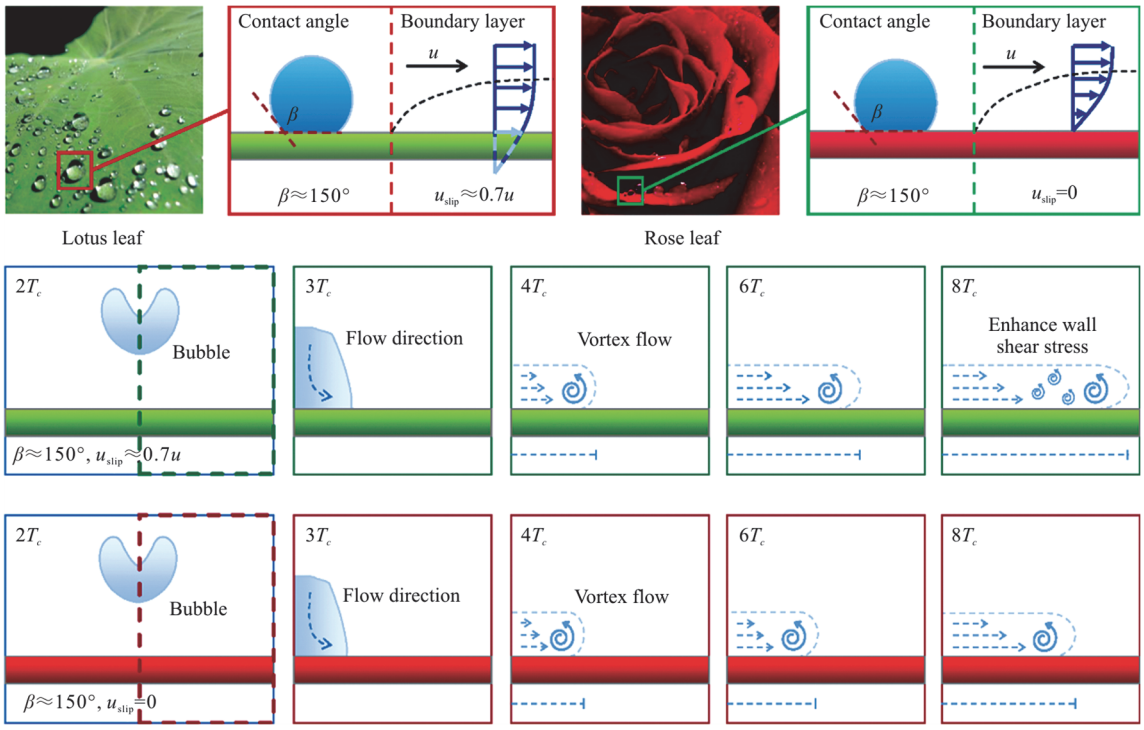

Fig. 4 (Color online) Schematic of the effects of wall wettability on vortex flows induced by collapses of cavitation bubble near a rigid wall[44]

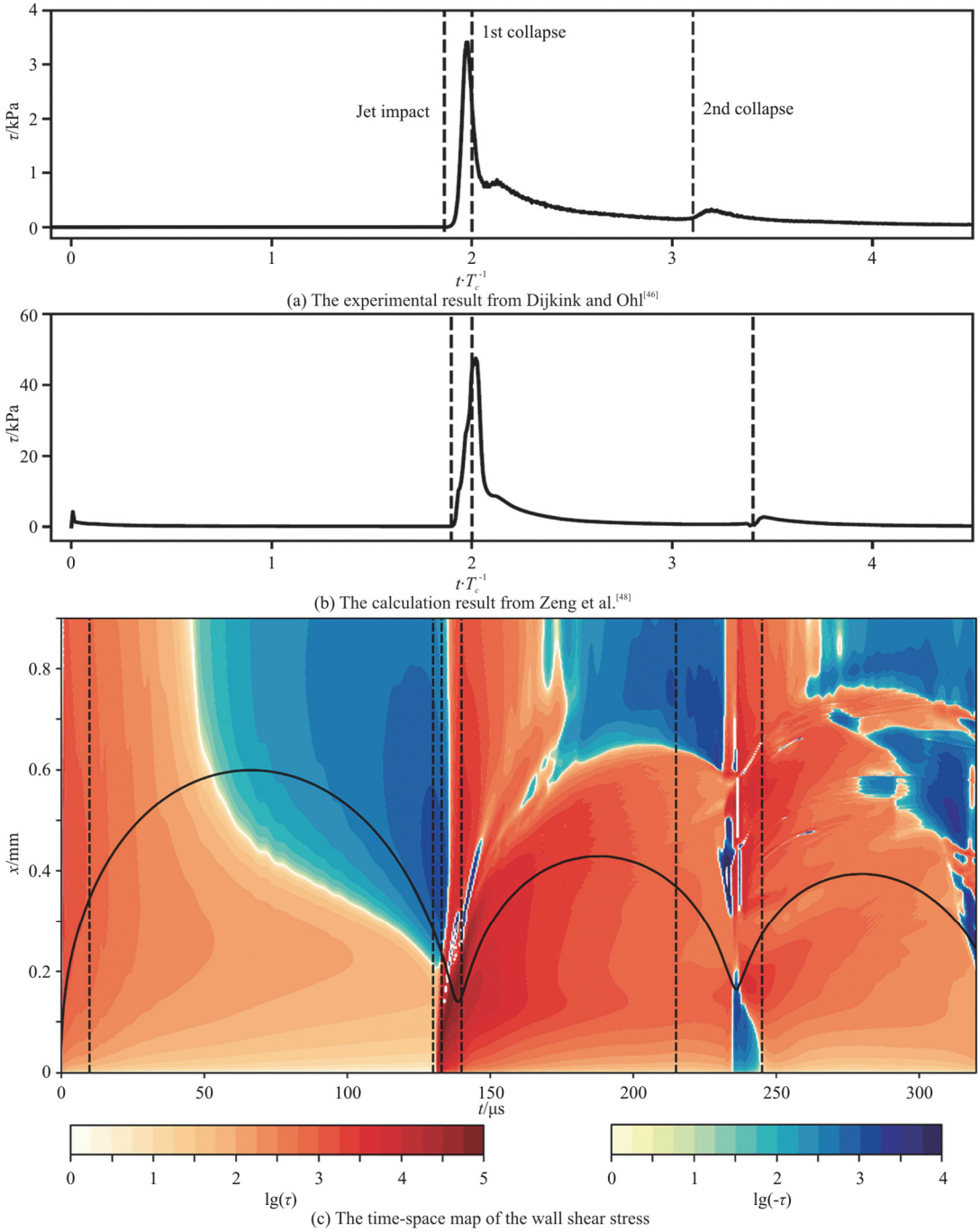

Fig. 5 (Color online) A measurement of the wall shear stress for a stand-off distance of $\gamma = 1.0$: (a) The experimental result from Dijkink and Ohl[46]. (b) The calculation result from Zeng et al.[48] and (c) The time-space map of the wall shear stress. In panels (a), (b), the horizontal axis is the dimensionless time normalized by the bubble collapse time

This method consisted of visualizing the corroded pit using an optical microscope and measuring the surface topography using a profilometer. Sarkar et al.[50] conducted a fluid-structure interaction simulation to analyze the mechanism of material deformation during cavitation bubble collapse. Combining an ultra-high-speed camera and an ex-situ measurement with confocal and scanning electron microscopy, Reuter et al.[35] proposed that an unexpected self-focusing mechanism might be the true reason for cavitation erosion. The regime of this self-focusing effect overlaps with the needle jet regime, i.e., it occurs only for $\gamma \leq 0.2$. In reality, the expanding and collapsing bubble is not perfectly axisymmetric, especially at a late stage, when the torus formed after jet impact collapses with a three-dimensional character. Indeed, the torus collapses progressively rather than all at once like in the axisymmetric case. The shockwaves

emitted by the gradually collapsing torus propagate and constructively superpose, leading to a maximum shockwave amplification, which then intensifies the collapse of the remaining bubble fragment and causes damage to the surface[50].

Cavitation erosion results in high costs, a reduction in energy efficiency, and the repair and downtime of damaged equipment such as ship propellers, water turbines, and cryogenic pumps[51-54]. Several strategies for mitigating cavitation erosion have been explored. Recently, Gonzalez-Avila[55] reported a method using biomimetic gas-entrapping microtextured surfaces. The entrapment of air inside the cavities repels cavitation bubbles from the surface, thereby preventing cavitation damage. Sun et al.[56] found that a surface containing gas can not only make the direction of motion of the microjet flow away from the wall, but can also shorten the oscillation period of cavitation compared with other wall surfaces[57]. Robles et al.[58] argued that the stability of entrapped air pockets is directly dependent on the hydrophobicity of surfaces and the number of incident cavitation cycles. Bubble dynamics have been recently explored for a cavitation bubble initiated near a rigid boundary with surface structures[27, 59-64]. These findings on the interaction between cavitation bubbles and surfaces with micro or macro structures provide new insights for mitigating cavitation erosion through the application of inexpensive and environmentally friendly materials.

1.1.5 Influences of liquid viscosity

The viscosity of the liquid affects the bubble dynamics near boundaries in two ways. First, the viscosity affects the overall flow field and, in particular, the boundary layer thickness, so that the characteristics of the bubble behaviors are changed, including the lifetime and the maximal size of the bubble, the shape and velocity of the jet, and the contact angle between the boundaries. The other change is in the value of the viscosity in the expression of the definition of the characteristics induced by the bubble collapse. For instance, the wall shear stress is defined as the product of the wall shear rate and the dynamic viscosity of the liquid. When a single bubble collapses near a rigid wall, it is further known that the viscosity has a significant influence on the bubble shape[65]. Furthermore, the very fast and thin jet observed in the study by Lechner et al.[30] is unlikely to be observed at a liquid viscosity 40 times higher than water as the annular inflow is no longer fast enough. At such high viscosities, a jet forms that is much wider and much slower (on the order of 100 m/s) than in water (about 1 000 m/s)[30]. Hupfeld et al.[66] presented experimental results for laser-induced bubbles using ultra-high-speed photography to study both the expansion and collapse phases in several liquids. They found that the viscosity of the liquid affects the growth, collapse, and bubble shapes, including the liquid microlayer and contact line evolution. Saini et al.[43] determined the maximum nondimensional velocity reached during the collapse as a function of the Reynolds number (see Fig. 6). When the Reynolds number is below this critical value, the jet velocity further drops dramatically, decaying with decreasing Re. This sudden change in the peak velocities is controlled by the appearance of jetting, which is not visible for $Re \le 100$. Zeng et al.[67] investigated the influence of the stand-off distance and liquid viscosity on the wall shear stress from jetting cavitation bubbles. Their simulations predicted a stronger wall shear stress for an inward flow with an increased viscosity, while for an outward flow, a local maximum wall shear stress was seen as the viscosity increased. Their work suggests that liquids with higher viscosities may provide an enhanced cleaning result, but an experimental exploration is needed.

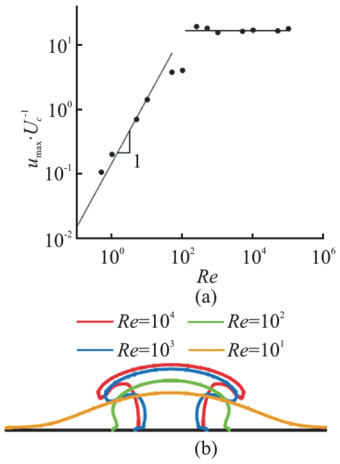

Fig. 6 (Color online) (a) The peak of the nondimensional velocity as a function of the Reynolds number for a bubble at $p_0 = 0.1$ atm collapsing in water at atmospheric pressure. (b) Interface contours as a function of the Reynolds number at the instant of minimum radius[43]

1.2 *Free surfaces*

Interactions between cavitation bubbles and free surfaces first drew the attention of researchers during World War II due to the potential to use surface deformation to defend surface ships from aircraft attacks[68]. Nowadays, this topic is widely investigated in the fields of underwater explosions[69-70], sea aerosol transportation[71-73], needle-free injections[74-76], and advanced inkjet printing[77-80]. Typically, small-scale cavitation bubbles are used to make qualitative observations to understand their interaction mechanisms[1, 81-85]. Under the constraint of a water surface, a bubble is repelled by the water surface when the re-entrant jet is oriented away from the water surface. The deformation of the water surface resulting from

the pulsation of an oscillating bubble is usually characterized by a splash sheet, breaking wrinkles, a spray water film, and a water spike.

1.2.1 Bubble dynamics

Chahine[86] was the first to obtain extraordinary images of the interaction between a cavitation bubble and a nearby free interface. The images captured the air-liquid interface deformation, which turned into a liquid "spike" jetting while the bubbles beneath moved and jetted away. They also found a critical value $\gamma = 3$ above which the oscillation of the bubble was not affected by the water surface. Blake and Gibson[87] also observed the toroidal collapse of a spark-induced bubble resulting from a re-entrant jet and compared their experimental result with theory. Since then, the jetting dynamics near a free surface have been extensively studied experimentally, theoretically, and numerically. Koukouvinis et al.[88] used numerical simulations to find that a jet with a mushroom cap formed during a collapse and split the initial bubble into an agglomeration of toroidal structures. Mushroom-shaped jets were clearly observed for the first time in front-light method experiments by Supponen et al.[89]. Supponen et al.[33] found that the jet formed during the collapse was broad and impacted the opposite bubble wall along a ring rather than at a single point $(\gamma = 1\text{-}3)$. Based on a combination of theoretical calculations and high-speed visualizations, jets can be classified into three distinct regimes–strong, intermediate, and weak–using an anisotropy parameter ζ [90]. The same analysis approach is also appropriate for analyzing bubble collapse near other surfaces such as rigid surfaces, inertial boundaries, and gravitational fields[91]. The anisotropy parameter ζ is derived based on the same consideration as the Kelvin impulse but in a dimensionless form. $\zeta = |\nabla p| R_0 / \Delta p$ is defined using the pressure gradient $|\nabla p|$, the maximal bubble radius R_0, and the driving pressure Δp. The normalized characteristics of the jets are approximated well by the power laws of ζ such as the jet impact time $(\sim 0.15\zeta^{5/3})$, jet speed $(\sim 0.9\zeta^{-1})$, bubble displacement $(\sim 2.5\zeta^{3/5})$, bubble volume at jet impact $(\sim 0.11\zeta^{2})$ and vapor-jet volume $(\sim 5.4\zeta)$), for the intermediate and weak jet regimes. However, as bubbles are seriously deformed in strong jet regimes, analysis with potential flow theory becomes inaccurate in these cases.

An example of the strong jet regime is shown in Fig. 7(a), in which a cavitation bubble is initially seeded a few microns below the free surface. The rapid expansion of the bubble produces a splash at the surface, and the cavitation bubble is exposed completely to the atmosphere, forming an open cavity[92-94]. The open cavity behaves very differently from the inertially collapsing cavitation bubble beneath a free surface, as was observed in previous reports[95]. Instead, the open cavity is first closed and then pierced by a liquid jet after the closure of the splash sheet. Both the cavity and the liquid jet travel away from the free surface and go considerably deeper into the pool. This jet is called a bullet jet to distinguish it from a regular jet[96]. The mechanism of the formation of bullet jets is similar to that of jets created by an object impacting a free surface[97-100], with the impact on the free surface leading to the formation of a deep and slender cavity in the liquid (see Fig. 7(b)). However, the content of the cavity can differ. In the cavity of a bullet jet, a small amount of the vapor bubble still remains, although the majority is entrapped air. While requiring the closure of an open cavity, a bullet jet only occurs in a narrow range of γ between 0.075 and 0.250. For an even smaller γ, as shown in Fig. 8[101], the splash sheet keeps propagating horizontally and does not seal, and as a result, a capillary wave is formed at the bubble surface and then propagates toward its bottom. Subsequently, a jet is generated and moves upward, which is similar to the so-called "Worthington jet"[19, 20, 102]. A qualitative description of the jet was first elucidated at the beginning of the twentieth century by Worthington[103-104]. Since then, jets emerging out of liquid interfaces have also been frequently observed in many other situations, such as in the bursting of surface bubbles[105-107].

The formation and collapse of a laser-induced cavitation bubble near a free surface is also accompanied by the emission of shock waves, which reflect at the air-water surface as rarefaction waves. These rarefaction waves bring tensile stress into the liquid, thus promoting the generation of secondary cavitation bubbles, as has been observed in many studies[88, 109-110]. This phenomenon was also used to seek bulk nanobubbles in a recent study by Rosselló and Ohl[111]. As illustrated in Fig. 9, a laser pulse was focused very close to the air-liquid interface to create a shock wave that reflected at the air-liquid surface into a tension wave. Once the tension wave reaches the region illuminated by a collimated pulse laser beam (seeding laser), small but oscillating cavitation bubbles are seen. As the seeding laser pulse has an intensity approximately 500 times lower than the reported intensity threshold for optical breakdown[112-113], these cavitation bubbles are likely the result of bulk existing nuclei being expanded by the tension wave. Using the Keller-Miksis equation, one can determine that these cavitation nuclei have initial radii of the order of 10 nm-100 nm, which proves that the illumination of

the seeding laser pulse produces bulk nanobubbles. This technique has been claimed to provide a higher degree of control over nano/microbubble production than other methods such as sudden decompression, liquid shaking, ultrasound, and electrolysis. However, debates on this subject are still ongoing.

1.2.2 Air-liquid interface jetting

The deformation of the liquid surface depends strongly on the stand-off distance γ. Chen et al.[115] investigated the morphology of the crown-like liquid film generated by a laser-induced bubble. They revealed that the crown formation is related to the surface

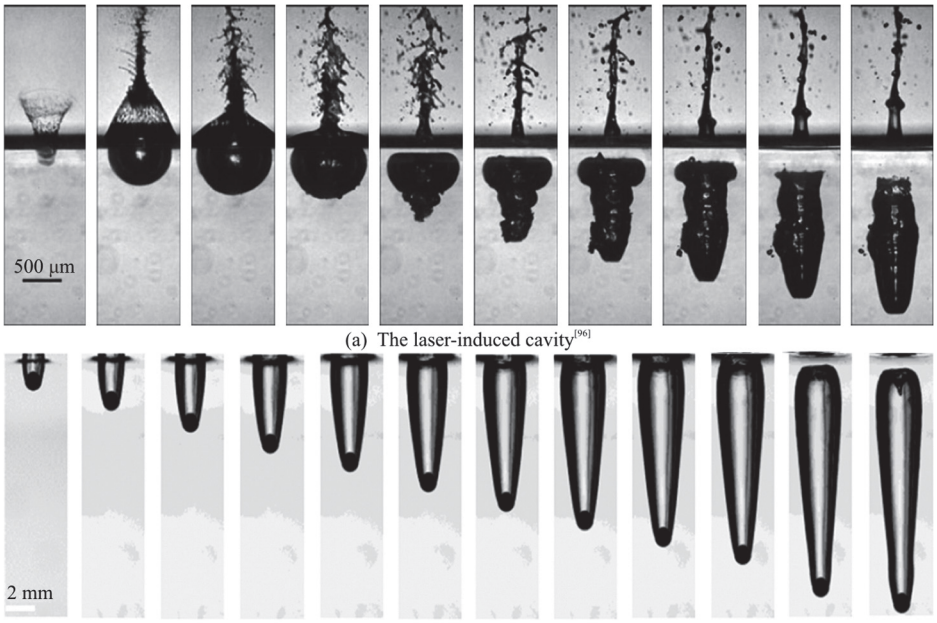

(a) The laser-induced cavity[96]

(b) The water-entry cavity[108]

Fig. 7 Experimental observation of the resulting "bullet" jet: (a) The laser-induced cavity[96], (b) The water-entry cavity[108]. The time intervals are 13.9 μs, 125 μs in cases (a), (b)

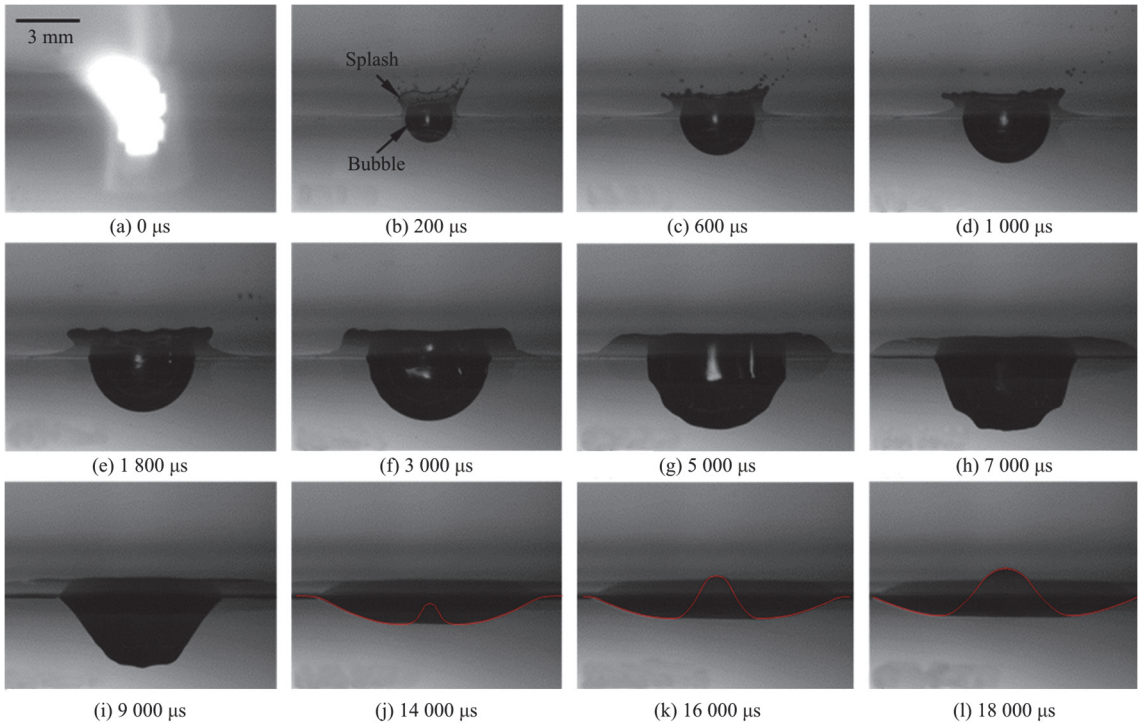

Fig. 8 (Color online) Experimental observation on the evolution of an open splash when an oscillating bubble bursts near a water surface at $\gamma = 0.02$ [101]

depression generated during bubble contraction. Zhang et al.[116] summarized six distinctive water surface patterns, including a special scenario in which a dome with a breaking liquid layer at the water surface was generated and a spark-induced bubble burst into the air at $\gamma = 0.45$. When γ was further reduced, the liquid was ejected from the free surface soon after the breakdown, i.e., the bubble burst into the air with the formation of a transparent splash. The splash first expanded both horizontally and vertically and then sealed for a narrow range with $0.075 < \gamma < 0.25$)[117]. Such a splash sheet is fundamentally important because it is related to many key problems and novel applications, such as aerosol formation at the sea surface, transmedium vehicles, liquid forward transfer, and needle-free injection. Similar dynamics have also been found in other phenomena related to the impact of solids, for instance, when an object impacts a quiescent water pool[118-123] or when a heavy sphere is dropped onto a bed of loose and fine sand[124]. Recently, many other investigations have been conducted to reveal different aspects of this problem. Marston et al.[125] observed the evolution of splash sheets under different ambient pressures. They argued that the suction from the rapid expansion of the oscillating bubble below the surface causes a closure of the splash. Rosselló et al.[96] observed that the closure of the splash sheet resulted in the generation of a slender and stable cavity with a bullet jet. They found that the closure of the water splash was provoked by a pressure difference between the cavity interior and the atmosphere, and also that the surface tension had an almost negligible influence on the splash dynamics. Wang et al.[101] proposed that bubble bursting is induced by a Rayleigh-Taylor instability. The mechanism behind this is demonstrated through a

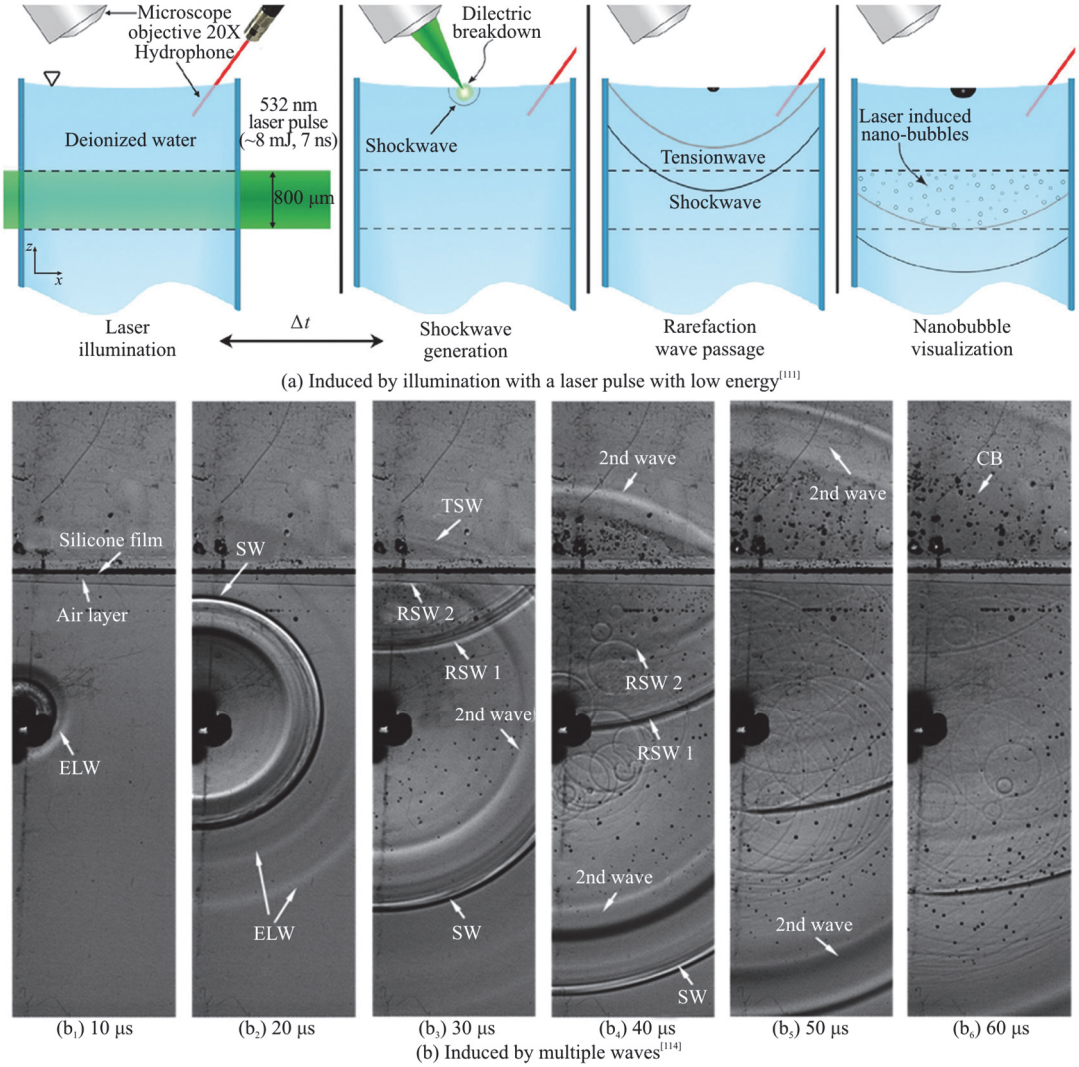

Fig. 9 (Color online) An observation of cavitation nucleation: (a) Induced by illumination with a laser pulse with low energy[111], (b) Induced by multiple waves[114]. In (b), multiple waves are generated by the underwater electric discharge with a 2 mm air layer. ELW: Elastic wave, SW: Shock wave, RSW1: The reflection of the shock wave, RSW2: The reflection of the second wave, TSW: The transition of the shock wave through the air layer, CBs: Cavitation bubbles

simulation in Fig. 10. During the early expansion of the bubble, some ripples are seen forming at the bubble's top surface. Although the bubble keeps expanding, its velocity is decreasing, i.e., the bubble surface is deaccelerating. Thus, the bubble surface is under a Rayleigh-Taylor type instability with an acceleration pointing downward[101]. As a result, the perturbed bubble surface grows. Meanwhile, the liquid between the bubble and air becomes thinner as the bubble expands. Finally, ventilation points are induced when the perturbed bubble surface touches the air-liquid surface. Although several studies have been conducted on the dynamics of the splash sheet induced by the burst of a cavitation bubble, many puzzles related to this complicated problem remain unanswered, for example, the stability of surfaces under dramatically different and transient accelerations induced by cavitation bubbles.

The laser-induced forward transfer (LIFT) is a digital printing technique that uses cavitation bubbles to transfer parts of a donor film to a receiving substrate. The process is shown in Figs. 11(a), 11(b). First, a laser pulse is deposited inside a film of liquid ink, and as the highly focused energy is absorbed by the ink, a cavitation bubble is formed due to either thermal or optical breakdown. The oscillating bubble induces a movement of the free surface, which finally leads to jet or hump formation depending on the deposited energy. LIFT can be adapted to different materials, varying from Newtonian fluid to complex liquids and biological materials, for inkjet printing, delivering liquid matter with precise control, and producing ultrafast thin jets for hypodermic injections[126]. A perfect LIFT process requires the formation of a clean and straight jet of ink that later deposits a single droplet on the receiver substrate. Figs. 11(c), 11(d) shows a comparison of jet generation under different input energies. The ejection of the jets involves two stages. In the first stage, the expansion and collapse of the cavitation bubble produce very thin (~10 μm) and fast (~10 m s^{-1}) jets, while in the second stage, a relatively thick (~100 μm) and slow (~1 m/s) jet is produced by the re-expansion of the bubble. The first jet can be utilized for high-resolution printing if the comparatively thicker second jet is avoided. However, the first jet is too thin to print functional materials with elements that are larger than the jet radius, such as emulsions with large suspensions and cells, which the second jet is potentially capable of producing[127]. Recently, quantitative analyses of the first and second jets have attracted increasing attention. Experiments have shown that the formation of a second jet is accompanied by a crown structure. Although some studies have argued that compressibility effects such as large pressure waves are responsible for the crown[128], explicitly incompressible simulations[129] that can reproduce the crown demonstrate have demonstrated compressibility is not essential to this phenomenon. Moreover, the effects of the shock waves produced by bubble collapse last for only a few microseconds before the formation of the second jet, and so are unlikely to induce significant motion of the surface[79]. A recent parametric study using an incompressible VoF simulation suggested that such a shock wave impinging on a surface has a limited effect on crown formation[130].

1.2.3 Liquid-liquid interface jetting

A liquid jet also forms between two different liquids when a cavitation bubble collapses near the

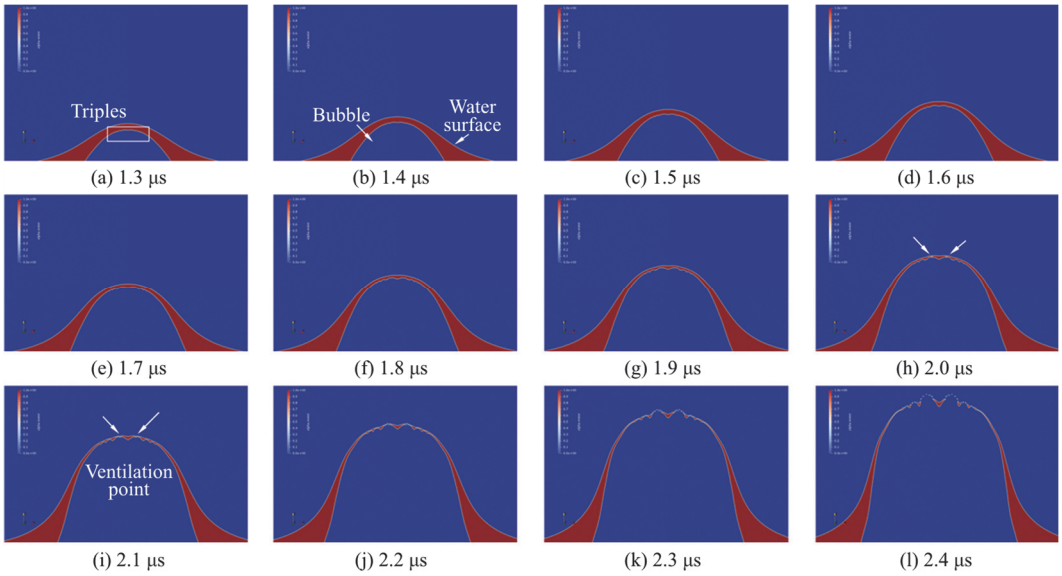

Fig. 10 (Color online) The process of a bubble bursting in extreme vicinity to a water surface at $\gamma = 0.15$. In the volume fraction field, blue and red represent the gas and liquid phases[101]

interface between them. Studies of such jets and the related bubble dynamics have originated from the demand for a comprehensive understanding of emulsion fabrication using ultrasound cavitation, as emulsions are indispensable in numerous fields, such as the food industry, pharmaceutical industry, cosmetic industry, and agriculture. The high-frequency acoustic irradiation (normally in the range of 0.02 MHz-1.00 MHz) in liquids produced by ultrasound devices generates so-called ultrasound cavitation, which also involves processes such as the formation, growth, and subsequent collapse of bubbles. Stepišnik Perdih et al.[132] found that rich phenomena occurred near the liquid–liquid interface when such a fluid system was exposed to ultrasound, including the oscillation of cavitation bubbles, the penetration of a water jet into the bulk oil phase, and the breakup of oil droplets. Yamamoto et al.[133] experimentally studied the dynamics of acoustic cavitation bubbles near a gallium droplet interface. They demonstrated that a high-speed liquid jet is the main cause of liquid emulsification and requires a large amplitude change in the bubble oscillation to trigger. To better understand the fundamental ultrasonic emulsification process, individual bubbles induced by laser or electric pulses are used for detailed investigations. Examples include the work of Orthaber et al.[134], who studied the jetting behavior of a laser-induced cavitation bubble (~1 mm) near a liquid-liquid interface, and Han et al.[135] who experimentally, numerically, and theoretically investigated the nonlinear interaction between a cavitation bubble and the interface of two immiscible fluids (oil and water) on multiple time scales. Figure 12 shows one of the experimental results, where a cavitation bubble is nucleated by an electric spark at the interface, with oil on top and water below. The authors showed that the difference in density causes the upper and lower parts of the bubble to undergo different collapse processes, which results in a downward jet aiming at the water part due to a faster contraction of the upper hemisphere. The authors explained that the viscous effect is limited, so the dynamics are still inertia-dominated, and the resulting phenomenon is a direct consequence of the

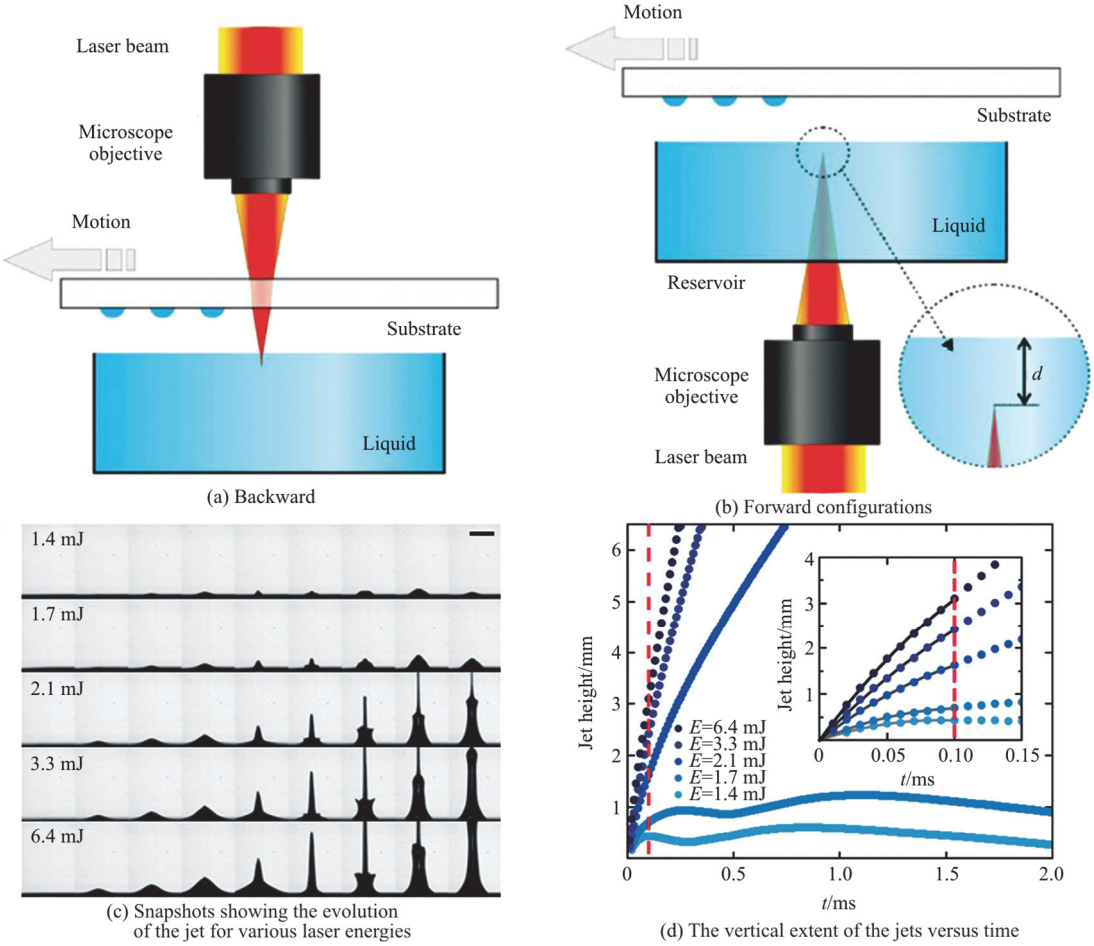

Fig. 11 (Color online) Schematics of film-free laser printing (FF-LIFT) The snapshots show the evolution of the jet for t = 0 ms, 0.01 ms, 0.02 ms, 0.05 ms, 0.10 ms, 0.18 ms, 0.33 ms, 0.61 ms, 1.10 ms and 2.00 ms. The scale bar corresponds to 2 mm. The inset shows a zoomed-in version of the region for the early stage of ejection[79, 131]

lower inertia of the oil.

1.3 *Elastic boundaries*

1.3.1 Bubble dynamics

Interest in interactions between cavitation bubbles and elastic boundaries has recently been revived because of the increasing number of relevant biomedical and biological applications of such interactions[109, 136-138]. Compared with a hard rigid boundary, the bubble dynamics near an elastic boundary are more complicated, as a deformable flow-structure coupling is involved. On the one hand, the oscillating bubble induces strong and transient hydraulic pressure and shear stresses acting on the elastic boundary, which causes boundary deformation. On the other hand, the deformed boundary severely affects the bubble dynamics, and a dominant feature is seen in which the formation of an annular jet leads to bubble splitting and the formation of two very fast axial jets directed in opposite directions[6, 139-141] as shown in Fig. 13. In addition to the stand-off distance between the bubble and the boundary, the elastic modulus and thickness of the boundary are the main parameters affecting the bubble dynamics.

Gibson[142] were the first to observe the bubble migration and the induced microjet traveling outward when a bubble expanded and collapsed near an elastic boundary. This unexpected phenomenon was then shown to prevent cavitation erosion, as the soft surface could repel the bubble and thus mitigate or even hinder jet impingement. Since then, the dynamics of bubbles have been investigated thoroughly with experiments and numerical simulations[2, 143-146]. One of the most comprehensive experimental studies was performed by Brujan et al.[147-149], who found that there was a large variation in both the jetting behavior and the deformation of the elastic boundary depending on the stand-off distance between the bubble and the boundary. In these initial experiments, the elastic boundaries were made of polyacrylamide (PAA) gels with different water concentrations and elastic moduli varying from 0.017 MPa to 2.030 MPa. This range covers the elastic properties of various biological tissues, such as the renal parenchyma (0.06 MPa), abdominal aorta (0.98-1.42 MPa), femoral artery (1.23 MPa-5.5 MPa), articular cartilage (0.43 MPa-1.15 MPa), muscle (0.06 MPa-0.8 MPa), and cornea (0.3 MPa-5 MPa). Yu et al.[150] found that a significant pressure difference between the elastic boundary and the underside of the bubble contributed to the formation of a "mushroom" bubble and inverted cone bubble through PIV using a commercial PIV system, but provided no PIV images. Xu et al.[151] investigated the effects of elastic moduli on bubble dynamics and found that a neck position appears on the upper part of the bubble as the elastic modulus of the material increases (see Fig.14). Sieber et al.[152] emphasized the strong dependence of bubble behaviors on the elasticity of the boundary, especially for the velocity and orientation of the microjet and the direction of bubble migration, using a combination of numerical simulations and experimental observations. Such microjets can reach supersonic velocities of up to 2 000 m/s, while the ensuing fully developed liquid microjet travels at average speeds of up to 1 000 m/s.

Recently, the effects of boundary thickness on bubble dynamics have attracted increasing attention. Zhai et al.[153] experimentally investigated the characteristics of the jets and shock waves of cavitation bubbles near elastic boundaries, focusing on the mechanism of cavitation erosion on elastic materials.

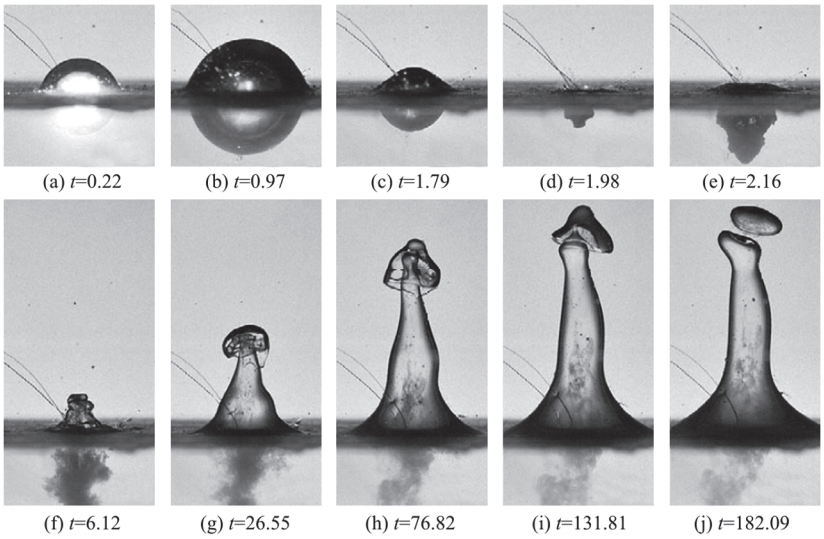

Fig. 12 An example of jetting at an oil-water interface produced by a spark cavitation bubble. The time is scale by 1.52 ms and each image has a width of 40 mm. The top part is oil and the lower part is water[135]

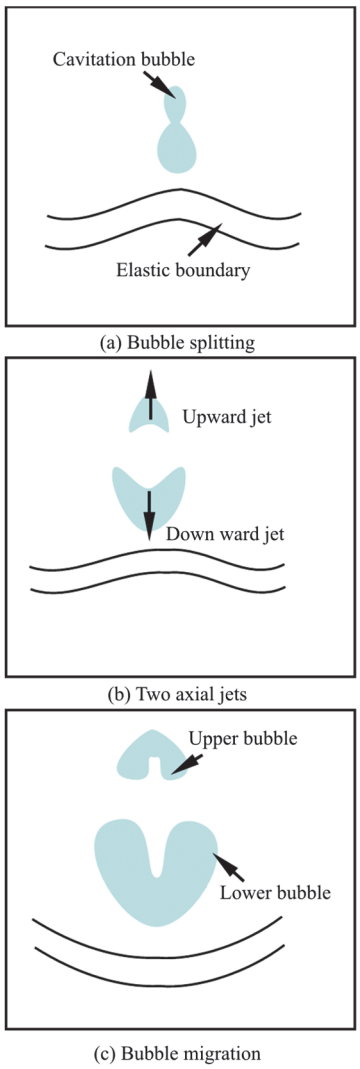

Fig. 13 (Color online) A schematic of a bubble splitting near an elastic boundary

They showed that the shock wave has a weak effect, and thus is unlikely to damage the materials, while microjet impingement on the surface can cause severe deformation of the elastic boundary and even ruptures. Kan et al.[154] analyzed the interactions between spark-induced cavitation bubbles and rubble sheets of different thicknesses. The experimental results showed that the sheet thickness was a dominant factor in determining the dynamics of the bubble, and the three jetting regimes and the rupture behavior were summarized with a parameter map consisting of the stand-off distance and the thickness of the elastic sheet. Wang et al.[155] analyzed the formation of two axial jets of cavitation bubbles near soft membranes with different thicknesses. They found that wrinkles in the membrane occurred during the contraction of the bubble when the thickness of the membrane was approximately 0.3 mm for bubbles with maximum radii $R_{\max} = 12.5 \pm 0.5$ mm . Lokar et al.[156] investigated cavitation bubble dynamics in the vicinity of a thin membrane wetted by different fluids on the other side. The results showed that the bubble dynamics could be tuned using liquids with various properties (mostly densities) and the membrane itself influenced the bubble dynamics less under this circumstance. Nowadays, with advanced experimental techniques and numerical methods, more of these features are still being revealed, but due to the complex nature of the problem and the many parameters involved, there are still open questions remaining, such as those concerning the bubble dynamics near an elastic sheet that vibrates at a high frequency.

1.3.2 Bubble-based techniques and their applications

The penetration of an elastic boundary induced by a jetting cavitation bubble has gained increasing attention due to its applications in bubble-based sonoporation and needle-free injection technologies. One can use sonoporation to directly deliver drug molecules into cells, using one or a combination of mechanisms among corresponding shear stress, inertially collapsing cavitation with microjets (inertial cavitation), and stable oscillating cavitation without jetting (stable cavitation). In biomedical applications, the bubbles are usually formed by injecting contrast agents, which are phase-change materials with lipid coatings that are excited using ultrasound. Two types of cavitation may occur, named stable cavitation and inertial cavitation. In stable cavitation, the push-and-pull effect during the expansion and compression stages can stimulate cellular messages to disturb the membrane integrity for a stable cavitation bubble[157], as shown in Fig. 15. When an inertial cavitation bubble occurs close enough to a cell membrane, the non-spherical bubble implosion results in a strong jetting flow (i.e., fluid streaming)[158-159], which can further rupture the membrane of an adjacent cell membrane. The inertial cavitation performance is dependent on many driving parameters of ultrasound cavitation, including the acoustic wave frequency, pulse duration, initial bubble radius, properties of the agents, temperature, fluid properties, function of the wave, and device energy efficiency. Apart from the effect of the jetting flow, shock waves generated from bubble collapse propagate and yield intense fluid streaming, resulting in the perforation of the membrane[160-162]. To the best of our knowledge, strong jetting flows and shock waves have a good chance of creating nonrecoverable cell membrane pores and causing low cell viability. Inertial cavitation also involves other unstable byproducts, such as high temperatures and reactive oxygen species, which could influence intracellular delivery and viability.

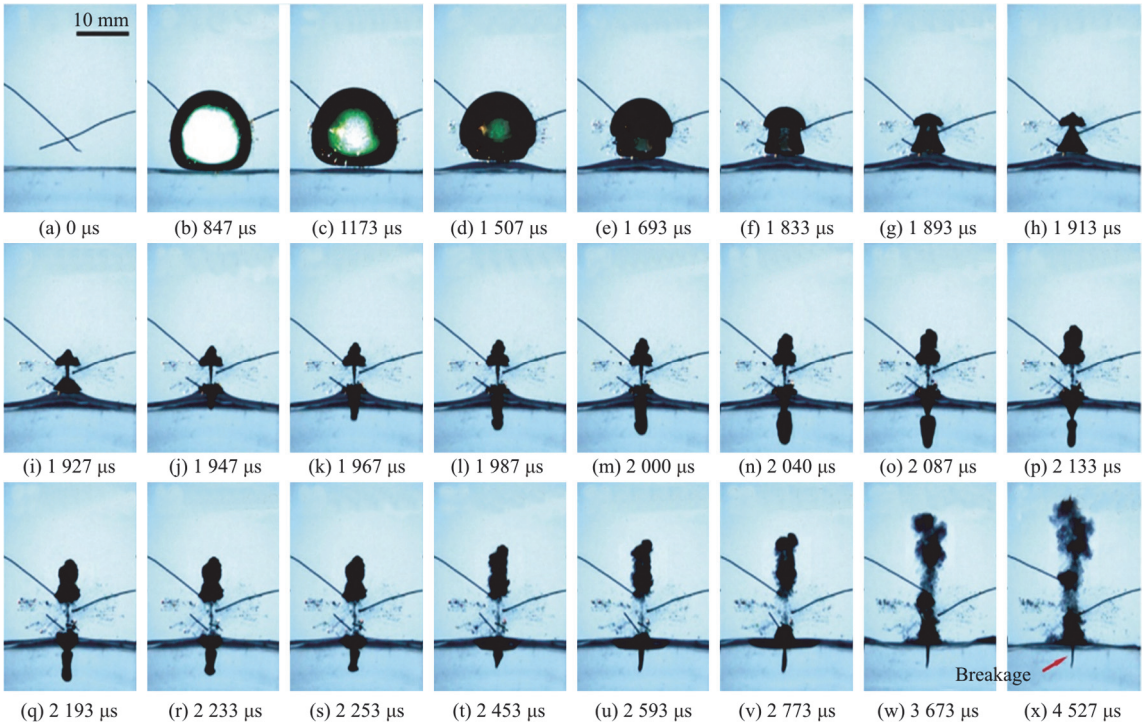

Fig. 14 (Color online) Cavitation erosion on an elastic boundary after the impact of a microjet ($R_{max} = 7.5$ mm , $\gamma = 0.78$)[151]

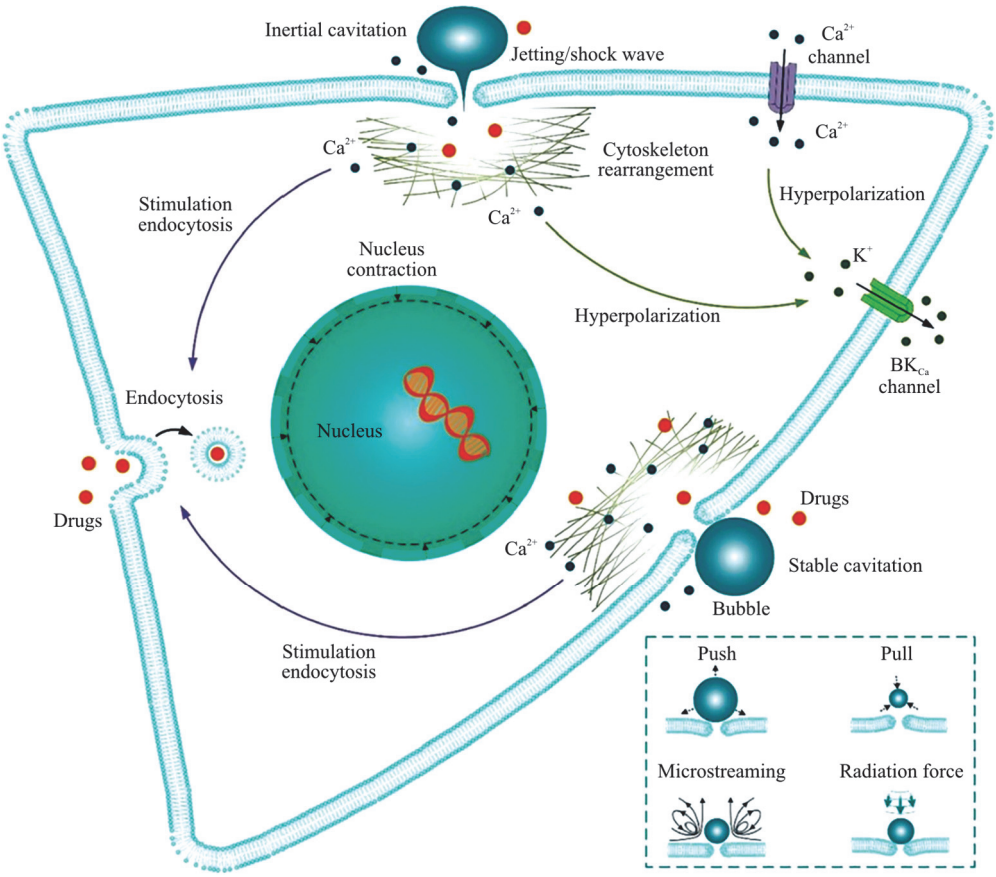

Fig. 15 (Color online) A schematic overview of major biophysical effects occurring during sonoporation generated by stable and inertial cavitation microbubbles[163]

Previously, needle-free injection techniques were based on the usage of a compressed spring or gas, which induced the sudden motion of a piston that could accelerate the liquid medication into a fast jet. Although some needle-free injectors have been released to the market, a previous study pointed out that the pain induced by these injectors is significantly greater than that induced by conventional needle injection, and their efficacy is less[164]. However, the concept has been renewed since cavitation bubbles were found to behave like on-demand micro-pumps to deliver liquid material by expanding and collapsing violently on a micro-scale. In the last decade, many studies have demonstrated that bubble-based needle-free injection is capable of generating fast and thin liquid jets that easily penetrate the skin and reach a sufficient depth[165-166]. In most implementations, laser-induced cavitation is used, as it is known to be the best method to precisely generate a bubble through an explosive phase change. The devices are generally designed in the following two ways. For the first and original design, the cavitation bubble is generated directly in the drug liquid to be injected[167-170] and in some cases directly next to the targeted soft material[171]. Another type of device is designed with two compartments next to each other. One of the compartments is for the liquid that absorbs the laser pulse energy to generate a cavitation bubble, while the other is a reservoir containing drug liquid. The two compartments are usually separated by a membrane or space that can vibrate. Mechanical interactions between liquid jets and body tissues, such as blood and tunica intima in blood vessels and cerebrospinal fluid and meninges in the brain, have been investigated widely and are responsible for possible damage and delivery efficiency. Several studies have reported on the potential of focused microjets in the development of a bubble-based needle-free injector with reduced pain and improved delivery efficiency[169]. The characteristics of the liquid jet, including the velocity, shape, and penetration site, have been widely analyzed through experimental observations, numerical simulations, and theoretical models (see Fig. 16)[172].

2. Jetting of cavitation bubbles between two parallel boundaries

A cavitation bubble collapsing in the vicinity of a large (semi-infinite) rigid wall experiences a pressure gradient pointing away from (toward) the wall. This gradient accelerates the wall-distant bubble surface and focuses nearby liquid through the shrinking and translating of the bubble toward the boundary. For a bubble with a sufficiently small distance, the liquid jet impacts perpendicularly onto the rigid wall and spreads radially. For more complex geometries, e.g., between two rigid boundaries or between a rigid boundary and a free surface, the pressure gradients of the individual boundaries superpose, and as a result, the bubble experiences richer dynamics and the flow is greatly altered.

While the bubble and the induced jet dynamics near a single solid boundary have been studied in great detail over the last half-century, bubble dynamics in thin gaps have been less explored. With the constriction of an additional solid boundary, a bubble may split into two daughter bubbles with two jets impacting both walls when the gap between the two walls is sufficiently small and the bubble nucleates near the gap center[173-179]. Gonzalez-Avila et al.[180] systemically investigated the bubble dynamics in a gap of variable height with two rigid walls. Three

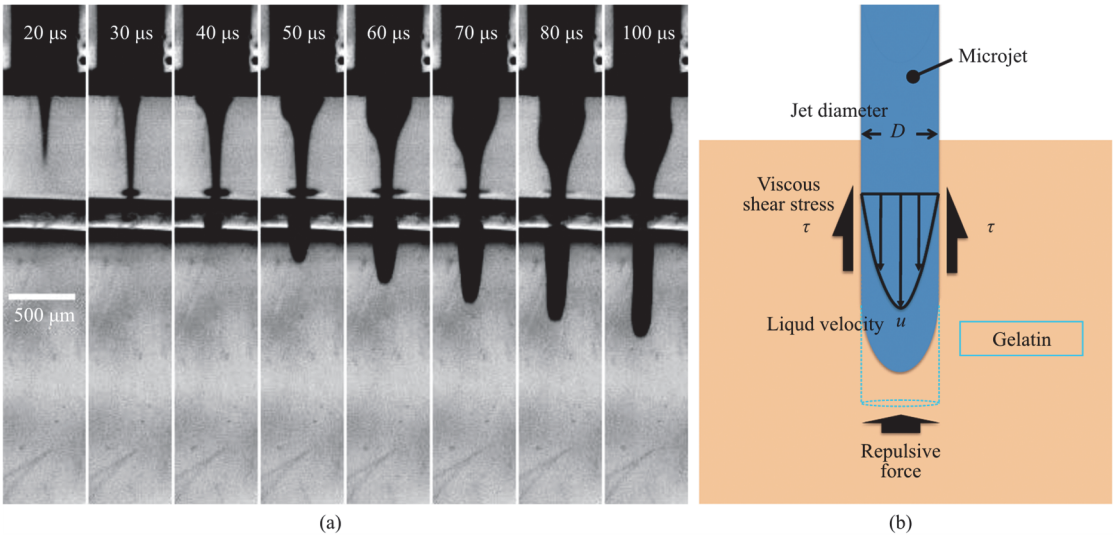

Fig. 16 (Color online) (a) Snapshots of jet penetration into gelatin, (b) A schematic sketch of the forces acting on the jet. In (b), the jet shown by the blue color penetrates into the gelatin[172]

scenarios were observed when the location of the bubble was fixed: neutral collapse at the gap center, collapse onto the lower wall, and collapse onto the upper wall (see Fig. 17). Han et al.[181] found that there are two conditions under which a bubble splits into two smaller bubbles, before collapsing toward the boundary closer to it and forming the corresponding liquid jets. Gonzalez-Avila et al.[182] studied the shear stress on both the proximal and distant plates and observed enhanced jet speed and shear stress compared with the case of cavitation bubbles near a single wall. Zeng et al.[183] summarized three different jetting scenarios that strongly depend on the stand-off distances of the bubble to the upper and lower walls and revealed detailed fluid mechanics by combing experiments and simulations. They pointed out that besides the vertically-inward flow developed from the bubble's top surface, two more flows are involved: The splitting flow due to the flow focusing effect at the center of the gap when the bubble shrinks, and the annular flow near the edge as a result of the inertial collapse of the most deformed region of the bubble. The competition between the three flows determines the jet dynamics. Rodriguez[184] used a numerical simulation to determine the role of confinement in the dynamics and wall impact loads of a cavitation bubble collapsing in a channel. Su et al.[185] found that the first pulsation periods of underwater explosion bubbles between two parallel plates are 30% to 50% higher than those in a free field. If the height of two rigid walls is further reduced to the order of micrometers, the configuration is similar to that of a Hele-Shaw cell and can be used to enable visualization of the movement of the fluid interface due to the nominally 2-D geometry[186-188].

When a cavitation bubble collapses between a rigid and a free surface, most of the motion features of the bubble and boundaries share some similarities with the single-boundary case. However, the main dynamics are changed, such as the jet speed and jet height[189]. The bubble also splits into two toroidal bubbles due to the same mechanism as that behind bubble collapses near a single free surface. Based on the configurations of the water spike, the free surface motions can also be categorized into five types, which are similar to the case of a single free surface. However, the induced jet is found to be much faster than that near a free surface, indicating that the jetting is strengthened when the bubble is nucleated between two boundaries with the same pressure gradient direction. The oscillation time is prolonged compared with the case of one free surface, but it is shortened compared with that in the case of a rigid wall. However, if the depth between the water surface and the rigid wall is reduced to the order of millimeters or even micrometers, the bubble dynamics differ substantially from the abovementioned studies. An example is shown in Fig. 18, in which after a bubble reaches its maximum size, an outward liquid jet begins to move away from the bubble while the bubble shrinks. The front velocity of the outward jet soon attains its maximum value, after which it decreases as the outward jet develops. The movement of the outward jet toward the receiver plate continues until it is disrupted by several bumps appearing on its free surface. The liquid jet subsequently breaks up to form droplets depending on the interplay among the inertial, capillary, and viscous effects for Newtonian fluids due to the Rayleigh-Plateau instability[18, 190-193]. Stable jets are much more easily produced in a wider range of fluences as the viscosity increases[194]. Therefore, several studies have shown that jet formation and stability are mainly related to the Ohnesorge dimensionless number, which relates the viscous

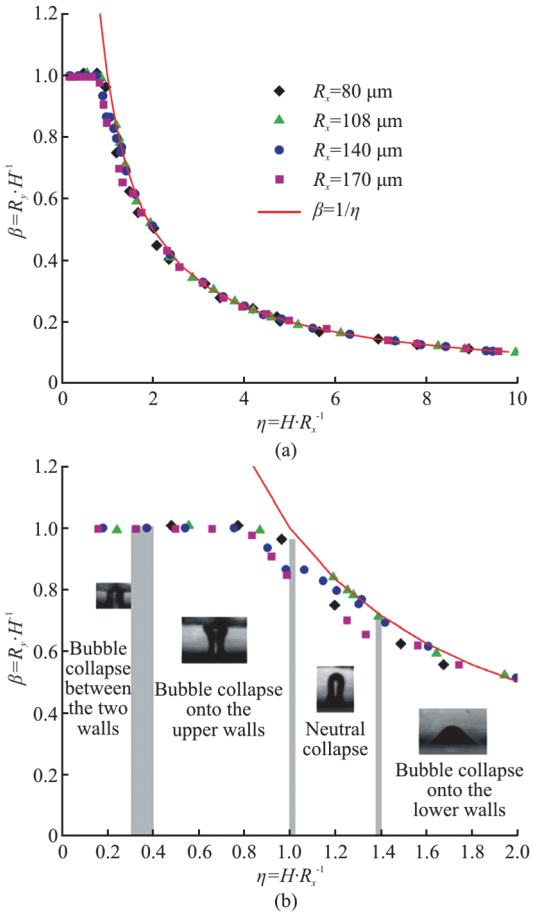

Fig. 17 (Color online) Cavitation bubble dynamics in a liquid gap of variable height: (a) A graph of the nondimensional bubble as a function of the nondimensional channel height, (b) An expanded view for small nondimensional channel heights revealing the non-hemispherical dynamics for four different bubble collapse regimes[180]

forces to the inertial and surface tension forces[195-198]. In addition, the energy of the laser plays a key role in the formation and stability of the jet[199].

It should be possible to identify new applications of cavitation by better understanding the bubble dynamics in other realistic geometries. Some studies have focused on the jetting behavior of a cavitation bubble collapsing near two perpendicular rigid walls[36, 201], in acute- or obtuse-angled corners[202-203], inside square and triangular channels[204], near the corner of a rigid wall and a free surface [205, 206], in a tube[207-209] and in a rectangular channel[210-211].

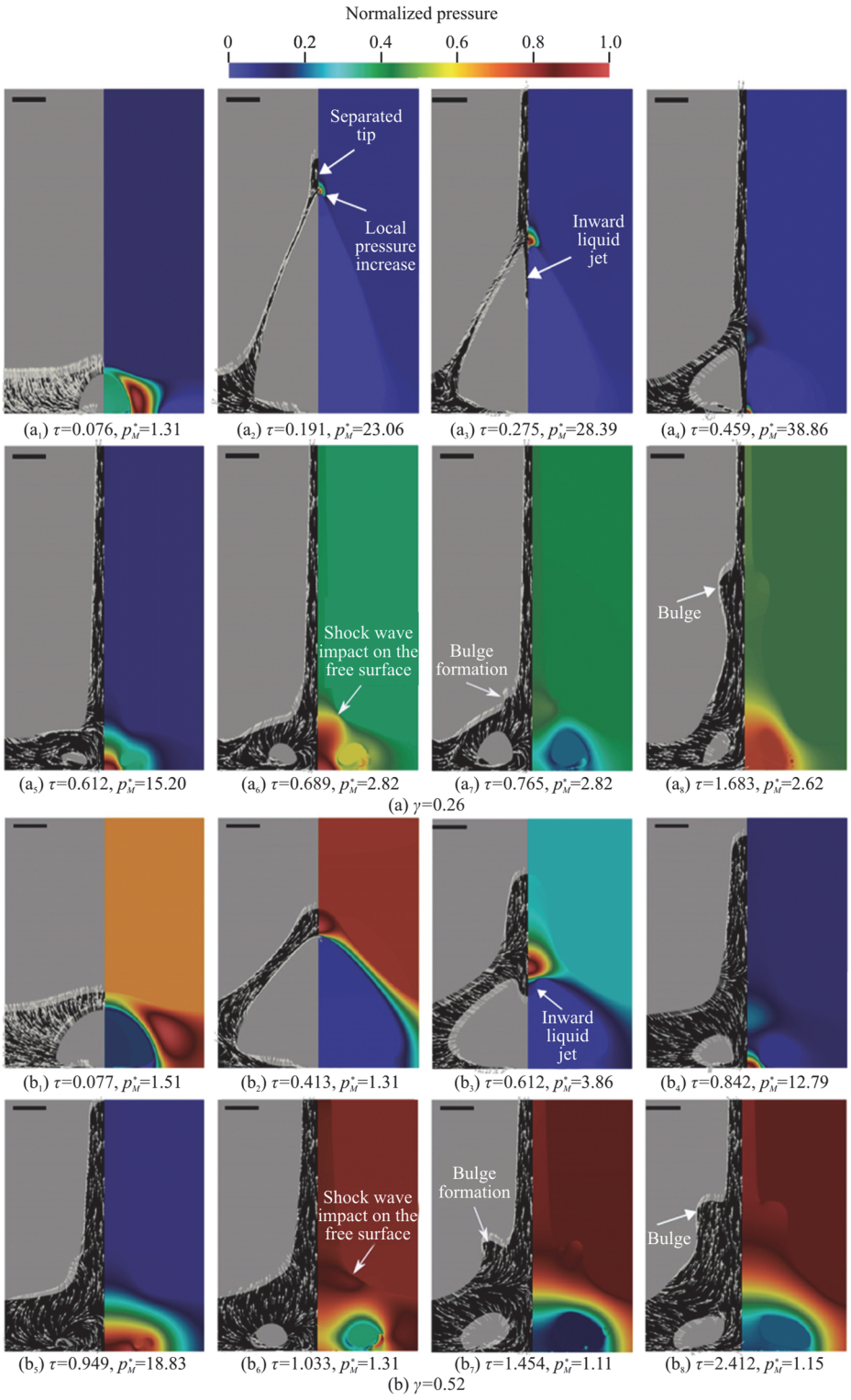

Fig. 18 (Color online) The normalized pressure (right) and velocity vectors (left). On the left side of each panel, the liquid and gas are represented by black and gray[200]

3. Summary and outlook

In this review, recent developments on the jetting dynamics of single cavitation bubbles near single boundaries and parallel boundaries have been summarized. In recent years, the cavitation phenomenon has been studied for bubbles collapsing extremely close to boundaries to provide new insights into potential engineering applications. A variety of promising developments are expected in the future. We see three directions that seem especially fruitful in view of the recent literature and the topics discussed in the 7th Cavitation and Multiphase Flows Workshop. This workshop, organized by the International Institute for Cavitation Research, was dedicated to various aspects of cavitation and multiphase flows realized across a wide range of applications.

First, the several oscillations of a bubble after the first collapse should receive more attention since the mechanical effects induced by the subsequent collapses may be more damaging to the nearby boundaries. One example is the case of cavitation erosion, in which the emitted shock pressure and wall shear stress after the first collapse can be more energetic as the residual bubble has moved closer. Second, further progress is expected in the description of the dynamic behaviors of micro- and nanobubbles near boundaries, especially elastic boundaries, due to an increasing interest from the biomedical engineering field. High-speed microphotography combined with surface measurements and high-resolution numerical simulations is currently lacking and should be explored. Finally, the hydrodynamic instabilities that occur during bubble collapse deserve to be better understood, especially at the stages of the final collapse and the interaction of liquid-gas interfaces, as the local instabilities of single cavitation bubbles may severely influence the stability of a cavitating multiphase flow, and more specifically, the occurrence and transition of turbulence in cavitating flows[212-213].

To achieve more inspiring progress on bubble-boundary interactions, the development of advanced theoretical, experimental, and numerical methods is required. Theoretical modeling is crucial to understanding the physics of bubbles under different conditions, which is the foundation for the utilization of bubbles and the circumvention of their hazardous effects. The models for multiple oscillations based on the Rayleigh-Plesset equation account for various effects, including boundaries, multiple bubbles, and external fields, but are demanding to develop. Recently, Zhang et al.[214] developed a novel theory to unify many classical equations for bubble dynamics, including the Rayleigh-Plesset, Gilmore, and Keller-Miksis equations, to predict bubble dynamics under miscellaneous conditions. This approach will also hopefully be applicable to circumstances with extremely small stand-off distances. The collapse of a single cavitation bubble involves multi-physical fields, such as fundamental physical processes taking place during the phase change between the liquid and vapor phases of a fluid and chemical reactions due to high internal pressures and temperatures at the collapse. Optical imaging has been widely employed to offer insight into the overall topology of a bubble during the whole oscillating process. To analyze accurately the collapse of a cavitation bubble, it is necessary to combine various measurement techniques, such as a high temporal-spatial-resolution spectroscope, pressure, and wall shear stress measurements. Reuter et al.[47] constructed a high-speed wall shear rate microscope for the spatiotemporal measurement of a rapid and transient wall shear flow. Synchronized high-speed imaging was used to record the behaviors of the bubble. Computational fluid dynamics (CFD) has recently increased in importance and accuracy, and is commonly used to produce quantitative predictions and to fill the knowledge gap left by regimes that are difficult to probe with experiments. We have also seen that the secondary development of open-source software can potentially be used to accurately simulate bubble collapse. OpenFOAM is one of the most popular software packages for CFD in the world. Zeng et al.[67] employed a compressible VOF approach for axisymmetric simulations in OpenFOAM to model the wall shear stress induced by cavitation bubbles. Furthermore, the problem of deformable flow-structure coupling can be solved by introducing the open-source software preCICE.

Acknowledgements

This work was supported by the Youth Innovation Promotion Association CAS (Grant No. 2022019), the High-level Innovation Research Institute Program of Guangdong Province (Grant Nos. 2020B0909010003, GARA2022002000).

Compliance with ethical standards

Conflict of interest: The authors declare that they have no conflict of interest. Jing-zhu Wang, Yi-wei Wang are editorial board members for the Journal of Hydrodynamics and was not involved in the editorial review, or the decision to publish this article. All authors declare that there are no other competing interests.

Ethical approval: This article does not contain any studies with human participants or animals performed by any of the authors.

Informed consent: Informed consent was obtained from all individual participants included in the study.

References

[1] Plesset M. S., Prosperetti A. Bubble dynamics and cavitation [J]. *Annual Review of Fluid Mechanics*, 1977, 9(1): 145-185.

[2] Blake J. R., Gibson D. C. Cavitation bubbles near boundaries [J]. *Annual Review of Fluid Mechanics*, 1987, 19(1): 99-123.

[3] Feng Z. C., Leal L. G. Nonlinear bubble dynamics [J]. *Annual Review of Fluid Mechanics*, 1997, 29: 201-243.

[4] Prosperetti A. Vapor bubbles [J]. *Annual Review of Fluid Mechanics*, 2017, 49: 221-248.

[5] Wang S. P., Zhang A. M., Liu Y. L. et al. Bubble dynamics and its applications [J]. *Journal of Hydrodynamics*, 2018, 30(6): 975-91.

[6] Dollet B., Marmottant P., Garbin V. Bubble dynamics in soft and biological matter [J]. *Annual Review of Fluid Mechanics*, 2019, 51: 331-355.

[7] Kornfeld M., Suvorov L. On the destructive action of cavitation [J]. *Journal of Applied Physics*, 1944, 15(6): 495-506.

[8] Plesset M. S., Chapman R. B. Collapse of an initially spherical vapour cavity in neighbourhood of a solid boundary [J]. *Journal of Fluid Mechanics*, 1971, 47: 283-290.

[9] Philipp A., Lauterborn W. Cavitation erosion by single laser-produced bubbles [J]. *Journal of Fluid Mechanics*, 1998, 361: 75-116.

[10] Shaw S. J., Schiffers W. P., Gentry T. P. et al. The interaction of a laser-generated cavity with a solid boundary [J]. *Journal of the Acoustical Society of America*, 2000, 107(6): 3065-3072.

[11] Zhang A. M., Yao X. L., Feng L. H. The dynamic behavior of a gas bubble near a wall [J]. *Ocean Engineering*, 2009, 36(3-4): 295-305.

[12] Li S., Li Y. B., Zhang A. M. Numerical analysis of the bubble jet impact on a rigid wall [J]. *Applied Ocean Research*, 2015, 50: 227-236.

[13] Zhang A. M., Li S., Cui J. Study on splitting of a toroidal bubble near a rigid boundary [J]. *Physics of Fluids*, 2015, 27(6): 062102.

[14] Reuter F., Zeng Q., Ohl C. D. The Rayleigh prolongation factor at small bubble to wall stand-off distances [J]. *Journal of Fluid Mechanics*, 2022, 944: A11.

[15] Lechner C., Lauterborn W., Koch M. et al. Fast, thin jets from bubbles expanding and collapsing in extreme vicinity to a solid boundary: A numerical study [J]. *Physical Review Fluids*, 2019, 4: 021601(R).

[16] Reuter F., Ohl C. D. Supersonic needle-jet generation with single cavitation bubbles [J]. *Applied Physics Letters*, 2021, 118(13): 134103.

[17] Lechner C., Lauterborn W., Koch M. et al. Jet formation from bubbles near a solid boundary in a compressible liquid: Numerical study of distance dependence [J]. *Physical Review Fluids*, 2020, 5(9): 093604.

[18] Eggers J., Villermaux E. Physics of liquid jets [J]. *Reports on Progress in Physics*, 2008, 71(3): 036601.

[19] Gekle S., Gordillo J. M. Generation and breakup of Worthington jets after cavity collapse. Part 1. Jet formation [J]. *Journal of Fluid Mechanics*, 2010, 663: 293-330.

[20] Yamamoto K., Motosuke M., Ogata S. Initiation of the Worthington jet on the droplet impact [J]. *Applied Physics Letters*, 2018, 112(9): 093701.

[21] Bokman G. T., Biasiori-Poulanges L., Lukic B. et al. High-speed x-ray phase-contrast imaging of single cavitation bubbles near a solid boundary [J]. *Physics of Fluids*, 2023, 35(1): 013322.

[22] Tong S. Y., Zhang S., Wang S. P. et al. Characteristics of the bubble-induced pressure, force, and impulse on a rigid wall [J]. *Ocean Engineering*, 2022, 255: 111484.

[23] Yang X., Liu C., Wan D. et al. Numerical study of the shock wave and pressure induced by single bubble collapse near planar solid wall [J]. *Physics of Fluids*, 2021, 33(7): 073311.

[24] Park S. H., Phan T. H., Park W. G. Numerical investigation of laser-induced cavitation bubble dynamics near a rigid surface based on three-dimensional fully compressible model [J]. *International Journal of Heat and Mass Transfer*, 2022, 191: 122853.

[25] Reuter F., Kaiser S. A. High-speed film-thickness measurements between a collapsing cavitation bubble and a solid surface with total internal reflection shadowmetry [J]. *Physics of Fluids*, 2019, 31(9): 097108.

[26] Tong S. Y., Zhang S., Wang S. P. et al. Characteristics of the bubble-induced pressure, force, and impulse on a rigid wall [J]. *Ocean Engineering*, 2022, 255: 111484.

[27] Luo J., Xu W., Zhai Y. et al. Experimental study on the mesoscale causes of the influence of viscosity on material erosion in a cavitation field [J]. *Ultrasonics Sonochemistry*, 2019, 59: 104699.

[28] Dular M., Delgosha O. C., Petkovsek M. Observations of cavitation erosion pit formation [J]. *Ultrasonics Sonochemistry*, 2013, 20(4): 1113-1120.

[29] Dular M., Pozar T., Zevnik J. et al. High speed observation of damage created by a collapse of a single cavitation bubble [J]. *Wear*, 2019, 418: 13-23.

[30] Lechner C., Lauterborn W., Koch M. et al. Jet formation from bubbles near a solid boundary in a compressible liquid: Numerical study of distance dependence [J]. *Physical Review Fluids*, 2020, 5(9): 093604.

[31] Blake J. R., Ohl C. D., Kurz T. et al. Bubble dynamics, shock waves and sonoluminescence [J]. *Philosophical Transactions of the Royal Society of London Series A: Mathematical, Physical and Engineering Sciences*, 1999, 357(1751): 269-94.

[32] Chahine G. L., Genoux P. F. Collapse of a cavitating vortex ring [J]. *Journal of Fluids Engineering*, 1983, 105(4): 400-405.

[33] Supponen O., Obreschkow D., Kobel P. et al. Shock waves from nonspherical cavitation bubbles [J]. *Physical Review Fluids*, 2017, 2(9): 093601.

[34] Gonzalez-Avila S. R., Denner F., Ohl C. D. The acoustic pressure generated by the cavitation bubble expansion and collapse near a rigid wall [J]. *Physics of Fluids*, 2021, 33(3): 032118.

[35] Reuter F., Deiter C., Ohl C. D. Cavitation erosion by shockwave self-focusing of a single bubble [J]. *Ultrasonics Sonochemistry*, 2022, 90:106131.

[36] Brujan E. A., Noda T., Ishigami A. et al. Dynamics of laser-induced cavitation bubbles near two perpendicular rigid walls [J]. *Journal of Fluid Mechanics*, 2018, 841: 28-49.

[37] Vogel A., Lauterborn W. Acoustic transient generation by laser-produced cavitation bubbles near solid boundaries [J]. *Journal of the Acoustical Society of America*, 1988, 84(2): 719-731.

[38] Fuster D., Dopazo C., Hauke G. Liquid compressibility effects during the collapse of a single cavitating bubble [J]. *Journal of the Acoustical Society of America*, 2011, 129(1): 122-131.

[39] Beig S. A., Aboulhasanzadeh B., Johnsen E. Temperatures

produced by inertially collapsing bubbles near rigid surfaces [J]. *Journal of Fluid Mechanincs*, 2018, 852: 105-125.
[40] Brujan E. A., Keen G. S., Vogel A. et al. The final stage of the collapse of a cavitation bubble close to a rigid boundary [J]. *Physics of Fluids*, 2002, 14(1): 85-92.
[41] Reuter F., Gonzalez-Avila S. R., Mettin R. et al. Flow fields and vortex dynamics of bubbles collapsing near a solid boundary [J]. *Physical Review Fluids*, 2017, 2(6): 064202.
[42] Sieber A. B., Preso D. B., Farhat M. Dynamics of cavitation bubbles near granular boundaries [J]. *Journal of Fluid Mechanics*, 2022, 947: A39.
[43] Saini M., Tanne E., Arrigoni M. et al. On the dynamics of a collapsing bubble in contact with a rigid wall [J]. *Journal of Fluid Mechanics*, 2022, 948: A45.
[44] Huang J., Wang J., Huang J. et al. Effects of wall wettability on vortex flows induced by collapses of cavitation bubbles: A numerical study [J]. *Physics of Fluids*, 2023, 35(8): 087122.
[45] Ohl C. D., Arora M., Dijkink R. et al. Surface cleaning from laser-induced cavitation bubbles [J]. *Applied Physics Letters*, 2006, 89(7): 074102.
[46] Dijkink R., Ohl C. D. Measurement of cavitation induced wall shear stress [J]. *Applied Physics Letters*, 2008, 93(25): 254107.
[47] Reuter F., Mettin R. Electrochemical wall shear rate microscopy of collapsing bubbles [J]. *Physical Review Fluids*, 2018, 3(6): 063601.
[48] Zeng Q., Gonzalez-Avila S. R., Dijkink R. et al. Wall shear stress from jetting cavitation bubbles [J]. *Journal of Fluid Mechanics*, 2018, 846: 341-55.
[49] Sagar H. J., El Moctar O. Dynamics of a cavitation bubble near a solid surface and the induced damage [J]. *Journal of Fluids and Structures*, 2020, 92: 102799.
[50] Sarkar P., Ghigliotti G., Franc J. P. et al. Mechanism of material deformation during cavitation bubble collapse [J]. *Journal of Fluids and Structures*, 2021, 105: 103327.
[51] Arabnejad M. H., Amini A., Farhat M. et al. Hydrodynamic mechanisms of aggressive collapse events in leading edge cavitation [J]. *Journal of Hydrodynamics*, 2020, 32(1): 6-19.
[52] Mohammadkhani A., Alizadeh M. Numerical prediction of hydrodynamic cavitating flow structures and their corresponding erosion [J]. *Journal of Hydrodynamics*, 2021, 33(3): 546-571.
[53] Liao H. L., Zhao S. L., Cao Y. F. et al. Erosion characteristics and mechanism of the self-resonating cavitating jet impacting aluminum specimens under the confining pressure conditions [J]. *Journal of Hydrodynamics*, 2020, 32(2): 375-384.
[54] Lei T. T., Cheng H. Y., Ji B. et al. Numerical assessment of the erosion risk for cavitating twisted hydrofoil by three methods [J]. *Journal of Hydrodynamics*, 2021, 33(4): 698-711.
[55] Gonzalez-Avila S. R., Dang Minh N., Arunachalam S. et al. Mitigating cavitation erosion using biomimetic gas-entrapping microtextured surfaces (GEMS) [J]. *Science Advances*, 2020, 6(13): eaax6192.
[56] Sun Y., Du Y., Yao Z. et al. The effect of surface geometry of solid wall on the collapse of a cavitation bubble [J]. *Journal of Fluids Engineering*, 2022, 144(7): 071402.
[57] Sun Y., Yao Z., Wen H. et al. Cavitation bubble collapse in a vicinity of a rigid wall with a gas entrapping hole [J]. *Physics of Fluids*, 2022, 34(7): 073314.
[58] Robles V., Gonzalez-Parra J. C., Cuando-Espitia N. et al. The effect of scalable PDMS gas-entrapping microstructures on the dynamics of a single cavitation bubble [J]. *Scientific Reports*, 2022, 12(1): 20379.
[59] Nott P. R. Boundary conditions at a rigid wall for rough granular gases [J]. *Journal of Fluid Mechanics*, 2011, 678: 179-202.
[60] Andrews E. D., Rivas D. F., Peters I. R. Cavity collapse near slot geometries [J]. *Journal of Fluid Mechanics*, 2020, 901: A29.
[61] Trummler T., Bryngelson S. H., Schmidmayer K. et al. Near-surface dynamics of a gas bubble collapsing above a crevice [J]. *Journal of Fluid Mechanics*, 2020, 899: A16.
[62] Aganin A. A., Kosolapova L. A., Malakhov V. G. Bubble dynamics near a locally curved region of a plane rigid wall [J]. *Physics of Fluids*, 2022, 34(9): 097105.
[63] Jiang N., Liu S., Chen D. Effect of roughness and wettability of silicon wafer in cavitation erosion [J]. *Chinese Science Bulletin*, 2008, 53(18): 2879-2885.
[64] Yuan H., Zhang J., Zhou J. et al. Study of wall wettability effects on cavitation bubble collapse using lattice Boltzmann method [J]. *AIP Advances*, 2021, 11(6): 065011.
[65] Gonzalez Avila S. R., Song C., Ohl C. D. Fast transient microjets induced by hemispherical cavitation bubbles [J]. *Journal of Fluid Mechanics*, 2015, 767: 31-51.
[66] Hupfeld T., Laurens G., Merabia S. et al. Dynamics of laser-induced cavitation bubbles at a solid-liquid interface in high viscosity and high capillary number regimes [J]. *Journal of Applied Physics*, 2020, 127(4): 044306.
[67] Zeng Q., An H., Ohl C. D. Wall shear stress from jetting cavitation bubbles: Influence of the stand-off distance and liquid viscosity [J]. *Journal of Fluid Mechanics*, 2022, 932: A14.
[68] Higdon C. E. Water barrier ship self defense lethality [J]. *Naval Engineers Journal*, 2000, 112(4): 121-35.
[69] Holt M. Underwater explosions [J]. *Annual Review of Fluid Mechanics*, 1977, 9(1): 187-214.
[70] Hung C. F., Hwangfu J. J. Experimental study of the behaviour of mini-charge underwater explosion bubbles near different boundaries [J]. *Journal of Fluid Mechanics*, 2010, 651: 55-80.
[71] Veron F. Ocean spray [J]. *Annual Review of Fluid Mechanics*, 2015, 47(1): 507-38.
[72] Lhuissier H., Villermaux E. Bursting bubble aerosols [J]. *Journal of Fluid Mechanics*, 2012, 696: 5-44.
[73] Berny A., Deike L., Séon T. et al. Role of all jet drops in mass transfer from bursting bubbles [J]. *Physical Review Fluids*, 2020, 5(3): 033605.
[74] Peters I. R., Tagawa Y., Oudalov N. et al. Highly focused supersonic microjets: Numerical simulations [J]. *Journal of Fluid Mechanics*, 2013, 719: 587-605.
[75] Mitragotri S. Current status and future prospects of needle-free liquid jet injectors [J]. *Nature Reviews Drug Discovery*, 2006, 5(7): 543-8.
[76] Delrot P., Modestino M. A., Gallaire F. et al. Inkjet printing of viscous monodisperse microdroplets by laser-induced flow focusing [J]. *Physical Review Applied*, 2016, 6(2): 024003.
[77] Brown M. S., Brasz C. F., Ventikos Y. et al. Impulsively actuated jets from thin liquid films for high-resolution printing applications [J]. *Journal of Fluid Mechanics*, 2012, 709: 341-70.
[78] Basaran O. A., Gao H., Bhat P. P. Nonstandard inkjets [J]. *Annual Review of Fluid Mechanics*, 2013, 45(1): 85-113.
[79] Jalaal M., Klein Schaarsberg M., Visser C. W. et al.

Laser-induced forward transfer of viscoplastic fluids [J]. *Journal of Fluid Mechanics*, 2019, 880: 497-513.
[80] Lohse D. Fundamental fluid dynamics challenges in inkjet printing [J]. *Annual Review of Fluid Mechanics*, 2022, 54(1): 349-82.
[81] Robinson P. B., Blake J. R., Kodama T. et al. Interaction of cavitation bubbles with a free surface [J]. *Journal of Applied Physics*, 2001, 89(12): 8225-37.
[82] Li S., Khoo B. C., Zhang A. M. et al. Bubble-sphere interaction beneath a free surface [J]. *Ocean Engineering*, 2018, 169: 469-83.
[83] Zhang A. M., Cui P., Cui J. et al. Experimental study on bubble dynamics subject to buoyancy [J]. *Journal of Fluid Mechanics*, 2015, 776: 137-60.
[84] Geng S., Yao Z., Zhong Q. et al. Propagation of shock wave at the cavitation bubble expansion stage induced by a nanosecond laser pulse [J]. *Journal of Fluids Engineering*, 2021, 143(1): 011501.
[85] Keller J., Kolodner I. Damping of underwater explosion bubble oscillation [J]. *Journal of Applied Physics*, 1956, 27: 1152-1161.
[86] Chahine G. L. Interaction between an oscillating bubble and a free surface [J]. *Journal of Fluids Engineering*, 1977, 99(4): 709-716.
[87] Blake J. R., Gibson D. C. Growth and collapse of a vapour cavity near a free surface [J]. *Journal of Fluid Mechanics*, 1981, 111: 123-140.
[88] Koukouvinis P., Gavaises M., Supponen O. et al. Simulation of bubble expansion and collapse in the vicinity of a free surface [J]. *Physics of Fluids*, 2016, 28(5): 052103.
[89] Supponen O., Kobel P., Obreschkow D. et al. The inner world of a collapsing bubble [J]. *Physics of Fluids*, 2015, 27(9): 091113.
[90] Supponen O., Obreschkow D., Tinguely M. et al. Scaling laws for jets of single cavitation bubbles [J]. *Journal of Fluid Mechanics*, 2016, 802: 263-293.
[91] Obreschkow D., Tinguely M., Dorsaz N. et al. Universal scaling law for jets of collapsing bubbles [J]. *Physical Review Letters*, 2011, 107(20): 204501.
[92] Vogel A., Venugopalan V. Mechanisms of pulsed laser ablation of biological tissues [J]. *Chemical Reviews*, 2003, 103(2): 577-644.
[93] Apitz I., Vogel A. Material ejection in nanosecond Er:YAG laser ablation of water, liver, and skin [J]. *Applied Physics A*, 2005, 81(2): 329-338.
[94] Thoroddsen S. T., Takehara K., Etoh T. G. et al. Spray and microjets produced by focusing a laser pulse into a hemispherical drop [J]. *Physics of Fluids,* 2009, 21(11): 112101.
[95] Pearson A., Cox E., Blake J. R. et al. Bubble interactions near a free surface [J]. *Engineering Analysis with Boundary Elements*, 2004, 28(4): 295-313.
[96] Rosselló J. M., Reese H., Ohl C. D. Dynamics of pulsed laser-induced cavities on a liquid–gas interface: From a conical splash to a 'bullet' jet [J]. *Journal of Fluid Mechanics*, 2022, 939: A35.
[97] Sun T., Wang H., Shi C. et al. Experimental study of the effects of a viscous liquid layer on the cavity dynamics of vertical entry by a sphere into water at low Froude number [J]. *Physics of Fluids*, 2021, 33(1): 013308.
[98] Hong Y., Zhao Z., Gong Z. et al. Cavity dynamics in the oblique water entry of a cylinder at constant velocity [J]. *Physics of Fluids*, 2022, 34(2): 021703.
[99] Wang Y., Wang Z., Du Y. et al. The mechanism of surface-seal splash during water entry [J]. *Physics of Fluids*, 2022, 34(4): 042110.
[100] Shi Y., Hua Y., Pan G. Experimental study on the trajectory of projectile water entry with asymmetric nose shape [J]. *Physics of Fluids*, 2020, 32(12): 122119.
[101] Wang G. H., Du Y., Xiao Z. J. et al. Numerical study on formation of a splash sheet induced by an oscillating bubble in extreme vicinity to a water surface [J]. *Journal of Hydrodynamics*, 2022, 34(5): 1021-1031.
[102] Bartolo D., Josserand C., Bonn D. Singular jets and bubbles in drop impact [J]. *Physical Review Letters*, 2006, 96(12): 124501.
[103] Worthington A. M., Cole R. S. Impact with a liquid surface studied by the aid of instantaneous photography. Paper II [J]. *Philosophical Transactions of the Royal Society of London Series A, Containing Papers of a Mathematical or Physical Character*, 1900, 194: 175-199.
[104] Du Y., Wang J. Z., Wang Z. Y. et al. The effect of gravity on self-similarity of Worthington jet after water entry of a two-dimensional wedge [J]. *Theoretical and Applied Mechnaincs Letters*, 2023, 13(5): 100462.
[105] Sanjay V., Lohse D., Jalaal M. Bursting bubble in a viscoplastic medium [J]. *Journal of Fluid Mechanics*, 2021, 922: A2.
[106] Gañán-Calvo A. M., López-Herrera J. M. On the physics of transient ejection from bubble bursting [J]. *Journal of Fluid Mechanics*, 2021, 929: A12.
[107] Constante-Amores C. R., Kahouadji L., Batchvarov A. et al. Dynamics of a surfactant-laden bubble bursting through an interface [J]. *Journal of Fluid Mechanics*, 2021, 911: A57.
[108] Zhong Y. X., Du Y., Qiu R. D. et al. Seal types of water-entry cavities generated by the impact of spheres with decreasing Bond number [J]. *Acta Mechanica Sinica*, 2023, 39: 322482.
[109] Požar T., Petkovšek R. Cavitation induced by shock wave focusing in eye-like experimental configurations [J]. *Biomedical Optics Express*, 2020, 11(1): 432-447.
[110] Supponen O., Obreschkow D., Kobel P. et al. Shock waves from nonspherical cavitation bubbles [J]. *Physical Review Fluids*, 2017, 2(9): 093601.
[111] Rossello J. M., Ohl C. D. On-demand bulk nanobubble generation through pulsed laser illumination [J]. *Physical Review Letters*, 2021, 127(4): 044502.
[112] Vogel A., Nahen K., Theisen D. et al. Plasma formation in water by picosecond and nanosecond Nd: YAG laser pulses. I. Optical breakdown at threshold and superthreshold irradiance [J]. *IEEE Journal of Selected Topics in Quantum Electronics*, 1996, 2(4): 847-60.
[113] Noack J., Vogel A. Laser-induced plasma formation in water at nanosecond to femtosecond time scales: Calculation of thresholds, absorption coefficients, and energy density [J]. *IEEE Journal of Quantum Electronics*, 1999, 35(8): 1156-67.
[114] Wang J., Abe A., Koita T. et al. Study of sterilization effects on marine Vibrio sp. using interaction of cavitation with shock wave in a narrow water chamber [J]. *Journal of Applied Physics*, 2018, 124(21): 213301.
[115] Chen R., Yu Y., Su K. W. et al. Exploration of water jet generated by Q-switched laser induced water breakdown with different depths beneath a flat free surface [J]. *Optics express*, 2013, 21: 445-453.
[116] Zhang S., Wang S. P., Zhang A. M. Experimental study on the interaction between bubble and free surface using a high-voltage spark generator [J]. *Physics of Fluids*, 2016, 28(3): 032109.
[117] Zhang A. M., Cui P., Wang Y. Experiments on bubble

dynamics between a free surface and a rigid wall [J]. *Experiments in Fluids*, 2013, 54(10): 1602.
[118] Duez C., Ybert C., Clanet C. et al. Making a splash with water repellency [J]. *Nature Physics*, 2007, 3: 180-183.
[119] Aristoff J. M., Bush J. W. M. Water entry of small hydrophobic spheres [J]. *Journal of Fluid Mechanics*, 2009, 619: 45-78.
[120] Bergmann R., van Der Meer D., Gekle S. et al. Controlled impact of a disk on a water surface: Cavity dynamics [J]. *Journal of Fluid Mechanics*, 2009, 633: 381-409.
[121] Marston J. O., Truscott T. T., Speirs N. B. et al. Crown sealing and buckling instability during water entry of spheres [J]. *Journal of Fluid Mechanics*, 2016, 794: 506-29.
[122] Eshraghi J., Jung S., Vlachos P. P. To seal or not to seal: The closure dynamics of a splash curtain [J]. *Physical Review Fluids*, 2020, 5(10): 104001.
[123] Yi L., Li S., Jiang H. et al. Water entry of spheres into a rotating liquid [J]. *Journal of Fluid Mechanics*, 2021, 912: R1.
[124] Royer J. R., Corwin E. I., Flior A. et al. Formation of granular jets observed by high-speed X-ray radiography [J]. *Nature Physics*, 2005, 1(3): 164-167.
[125] Marston J., Mansoor M., Thoroddsen S. et al. The effect of ambient pressure on ejecta sheets from free-surface ablation [J]. *Experiments in Fluids*, 2016, 57: 61.
[126] Mézel C., Souquet A., Hallo L. et al. Bioprinting by laser-induced forward transfer for tissue engineering applications: Jet formation modeling [J]. *Biofabrication*, 2010, 2(1): 014103.
[127] Cerbus R. T., Chraibi H., Tondusson M. et al. Experimental and numerical study of laser-induced secondary jetting [J]. *Journal of Fluid Mechanics*, 2022, 934: A14.
[128] Kiyama A., Tagawa Y., Ando K. et al. Effects of a water hammer and cavitation on jet formation in a test tube [J]. *Journal of Fluid Mechanics*, 2016, 787: 224-36.
[129] Liu N. N., Cui P., Ren S. F. et al. Study on the interactions between two identical oscillation bubbles and a free surface in a tank [J]. *Physics of Fluids*, 2017, 29(5): 052104.
[130] Saade Y., Jalaal M., Prosperetti A. et al. Crown formation from a cavitating bubble close to a free surface [J]. *Journal of Fluid Mechanics*, 2021, 926: A5.
[131] Serra P., Piqué A. Laser-induced forward transfer: Fundamentals and applications [J]. *Advanced Materials Technologies*, 2019, 4(1): 1800099.
[132] Stepišnik Perdih T., Zupanc M., Dular M. Revision of the mechanisms behind oil-water (O/W) emulsion preparation by ultrasound and cavitation [J]. *Ultrasonics Sonochemistry*, 2019, 51: 298-304.
[133] Yamamoto T., Matsutaka R., Komarov S. V. High-speed imaging of ultrasonic emulsification using a water-gallium system [J]. *Ultrasonics Sonochemistry*, 2021, 71: 105387.
[134] Orthaber U., Zevnik J., Petkovšek R. et al. Cavitation bubble collapse in a vicinity of a liquid-liquid interface-Basic research into emulsification process [J]. *Ultrasonics Sonochemistry*, 2020, 68: 105224.
[135] Han R., Zhang A. M., Tan S. et al. Interaction of cavitation bubbles with the interface of two immiscible fluids on multiple time scales [J]. *Journal of Fluid Mechanics*, 2022, 932: A8.
[136] Li S., Zhang A. M., Han R. Counter-jet formation of an expanding bubble near a curved elastic boundary [J]. *Physics of Fluids*, 2018, 30(12): 121703.
[137] Vogel A. Nonlinear absorption: Intraocular microsurgery and laser lithotripsy [J]. *Physics in Medicine and Biology*, 1997, 42(5): 895-912.
[138] Yuan F., Yang C., Zhong P. Cell membrane deformation and bioeffects produced by tandem bubble-induced jettiing flow [J]. *Proceddings of The National Academy of Sciences of the United States of America*, 2015, 112(51): E7039-47.
[139] Brinkmann R., Theisen D., Brendel T. et al. Single-pulse 30-J holmium laser for myocardial revascularization - A study on ablation dynamics in comparison to CO2 laser-TMR [J]. *IEEE Journal of Selected Topics in Quantum Electronics*, 1999, 5(4): 969-980.
[140] Klaseboer E., Khoo B. C. An oscillating bubble near an elastic material [J]. *Journal of Applied Physics*, 2004, 96(10): 5808-5818.
[141] Shervani-Tabar M. T., Aghdam A. H., Khoo B. C. et al. Numerical analysis of a cavitation bubble in the vicinity of an elastic membrane [J]. *Fluid Dynamics Research*, 2013, 45(5): 055503.
[142] Gibson D. C. Cavitation adjacent to plane boundaries [J]. *The 3rd Australasian Conf on Hydraulics and Fluid Mechanics*, Sydney, Australia, 1968, 210-214.
[143] Doinikov A. A., Aired L., Bouakaz A. Acoustic scattering from a contrast agent microbubble near an elastic wall of finite thickness [J]. *Physics in Medicine and Biology*, 2011, 5(21): 6951-6966.
[144] Gibson D. C., Blake J. R. The growth and collapse of bubbles near deformable surfaces [J]. *Applied Scientific Research*, 1982, 38: 215-224.
[145] Tomita Y., Kodama T. Interaction of laser-induced cavitation bubbles with composite surfaces [J]. *Journal of Applied Physics*, 2003, 94(5): 2809-2816.
[146] Shima A., Tomita Y., Gibson D. C. et al. The growth and collapse of cavitation bubbles near composite surfaces [J]. *Journal of Fluid Mechanics*, 1989, 203: 199-214.
[147] Brujan E., Nahen K., Schmidt P. et al. Dynamics of laser-induced cavitation bubbles near an elastic boundary [J]. *Journal of Fluid Mechanics*, 2001, 433: 251-281.
[148] Brujan E. A., Nahen K., Schmidt P. et al. Dynamics of laser-induced cavitation bubbles near elastic boundaries: Influence of the elastic modulus [J]. *Journal of Fluid Mechanics*, 2001, 433: 283-314.
[149] Brujan E. A., Nahen K., Schmidt P. et al. Dynamics of laser-induced cavitation bubbles near an elastic boundary used as a tissue phantom [C]. *proceedings of the 15th International Symposium on Nonlinear Acoustics*, Gottingen, Germany, 1999.
[150] Yu Q., Xu Z., Zhao J. et al. PIV-based acoustic pressure measurements of a single bubble near the elastic boundary [J]. *Micromachines*, 2020, 11(7): 637.
[151] Xu W., Zhai Y., Luo J. et al. Experimental study of the influence of flexible boundaries with different elastic moduli on cavitation bubbles [J]. *Experimental Thermal and Fluid Science*, 2019, 109: 109897.
[152] Sieber A. B., Preso D. B., Farhat M. Cavitation bubble dynamics and microjet atomization near tissue-mimicking materials [J]. *Physics of Fluids*, 2023, 35(2): 027101.
[153] Zhai Y., Xu W., Luo J. et al. Experimental study on the characteristics of microjets and shock waves of cavitation bubbles near elastic boundaries [J]. *Ocean Engineering*, 2022, 257.
[154] Kan X. Y., Yan J. L., Li S. et al. Rupture of a rubber sheet by a cavitation bubble: an experimental study [J]. *Acta Mechanica Sinica*, 2021, 37(10): 1489-1497.

[155] Wang A., Zhong. X., Wang G. H. et al. Experimental study on the formation of two axial jets of cavitation bubbles near soft membranes with different thicknesses [J]. *AIP Advances*, 2022, 12(9): 095023.
[156] Lokar Z., Petkovsek R., Dular M. Cavitation bubble dynamics in a vicinity of a thin membrane wetted by different fluids [J]. *Scientific Reports*, 2021, 11(1): 3506.
[157] Rich J., Tian Z., Huang T. J. Sonoporation: Past, present, and future [J]. *Advanced Materials Technologies*, 2022, 7(1): 2100885.
[158] Blake J. R., Keen G. S., Tong R. P. et al. Acoustic cavitation: the fluid dynamics of non-spherical bubbles [J]. *Philosophical Transactions of the Royal Society A-Mathematical Physical and Engineering Sciences*, 1999, 357(1751): 251-67.
[159] Ohl C. D., Arora M., Ikink R. et al. Sonoporation from jetting cavitation bubbles [J]. *Biophysical Journal*, 2006, 91(11): 4285-4295.
[160] Kodama T., Takayama K. Dynamic behavior of bubbles during extracorporeal shock-wave lithotripsy [J]. *Ultrasound in Medicine and Biology*, 1998, 24(5): 723-738.
[161] Helfield B. L., Chen X., Qin B. et al. Mechanistic insight into sonoporation with ultrasound-stimulated polymer microbubbles[J]. *Ultrasound in Medicine and Biology*, 2017, 43(11): 2678-2689.
[162] Postema M., van Wamel A., Lancee C. T. et al. Ultrasound-induced encapsulated microbubble phenomena [J]. *Ultrasound in Medicine and Biology*, 2004, 30(6): 827-840.
[163] Yang Y., Li Q., Guo X. et al. Mechanisms underlying sonoporation: Interaction between microbubbles and cells [J]. *Ultrasonics Sonochemistry*, 2020, 67: 105096.
[164] Harding L. M., Adeniyi A., Everson R. et al. Comparison of a needle-free high-pressure injection system with needle-tipped injection of intracavernosal alprostadil for erectile dysfunction [J]. *International Journal of Impotence Research*, 2002, 14(6): 498-501..
[165] Schoppink J., Fernandez Rivas D. Jet injectors: Perspectives for small volume delivery with lasers [J]. *Advanced Drug Delivery Reviews*, 2022, 182: 114109.
[166] Rossello J. M., Ohl C. D. Bullet jet as a tool for soft matter piercing and needle-free liquid injection [J]. *Biomedical Optics Express*, 2022, 13(10): 5202-5211.
[167] Oyarte Galvez L., Fraters A., Offerhaus H. L. et al. Microfluidics control the ballistic energy of thermocavitation liquid jets for needle-free injections [J]. *Journal of Applied Physics*, 2020, 127(10): 104901.
[168] Robles V., Gutierrez-Herrera E., Devia-Cruz L. F. et al. Soft material perforation via double-bubble laser-induced cavitation microjets [J]. *Physics of Fluids*, 2020, 32(4): 042005.
[169] Rohilla P., Marston J. Feasibility of laser induced jets in needle free jet injections [J]. *International Journal of Pharmaceutics*, 2020, 589: 119714.
[170] Krizek J., Lavickova B., Moser C. Degradation study on molecules released from laser-based jet injector [J]. *International Journal of Pharmaceutics*, 2021, 602: 120664.
[171] Mur J., Agrez V., Petelin J. et al. Microbubble dynamics and jetting near tissue-phantom biointerfaces [J]. *Biomedical Optics Express*, 2022, 13(2): 1061-1069.
[172] Tagawa Y., Oudalov N., El Ghalbzouri A. et al. Needle-free injection into skin and soft matter with highly focused microjets [J]. *Lab Chip*, 2013, 13(7): 1357-1363.
[173] Chahine G. L. Experimental and asymptotic study of non-spherical bubble collapse [J]. *Applied Scientific Research*, 1982, 38: 187-197.
[174] Kucherenko V. V., Shamko V. V. Dynamics of electric-explosion cavities between two solid parallel walls [J]. *Journal of Applied Mechanics and Technical Physics*, 1986, 27(1): 112-115.
[175] Sagar H. J., Moctar O. E. Dynamics of a cavitation bubble between oblique plates [J]. *Physics of Fluids*, 2022, 35(1): 013324.
[176] Ibn Azam F., Karri B., Ohl S. W. et al. Dynamics of an oscillating bubble in a narrow gap [J]. *Physical Review E*, 2013, 88(4): 043006.
[177] Liu B., Cai J., Huai X. Heat transfer with the growth and collapse of cavitation bubble between two parallel heated walls [J]. *International Journal of Heat and Mass Transfer*, 2014, 78: 830-838.
[178] Han B., Zhu R. H., Guo Z. Y. et al. Control of the liquid jet formation through the symmetric and asymmetric collapse of a single bubble generated between two parallel solid plates [J]. *European Journal of Mechanics/B fluids*, 2018, 72: 114-122.
[179] Zhang A. M., Ni B. Y., Song B. Y. et al. Numerical simulation of bubble breakup phenomena in a narrow flow field [J]. *Applied Mathematics and Mechanics (English Edition)*, 2010, 31(4): 449-60.
[180] Gonzalez-Avila S. R., Klaseboer E., Khoo B. C. et al. Cavitation bubble dynamics in a liquid gap of variable height [J]. *Journal of Fluid Mechanics*, 2011, 682: 241-260.
[181] Han B., Zhu R., Guo Z. et al. Control of the liquid jet formation through the symmetric and asymmetric collapse of a single bubble generated between two parallel solid plates [J]. *European Journal of Mechanics B-Fluids*, 2018, 72: 114-122.
[182] Gonzalez-Avila S. R., van Blokland A. C., Zeng Q. et al. Jetting and shear stress enhancement from cavitation bubbles collapsing in a narrow gap [J]. *Journal of Fluid Mechanics*, 2020, 884: A23.
[183] Zeng Q., Gonzalez-Avila S. R., Ohl C. D. Splitting and jetting of cavitation bubbles in thin gaps [J]. *Journal of Fluid Mechanics*, 2020, 896: A28.
[184] Rodriguez M., Jr., Beig S. A., Barbier C. N. et al. Dynamics of an inertially collapsing gas bubble between two parallel, rigid walls [J]. *Journal of Fluid Mechanics*, 2022, 946: A43.
[185] Su B., Yao X., Cui X. Experimental research of underwater explosion bubble dynamics between two parallel plates with various distances [J]. *Applied Ocean Research*, 2022, 122: 103081.
[186] Wang J., Li H., Guo W. et al. Rayleigh–Taylor instability of cylindrical water droplet induced by laser-produced cavitation bubble [J]. *Journal of Fluid Mechanics*, 2021, 919: A42.
[187] Zhao M., Niroobakhsh Z., Lowengrub J. et al. Nonlinear limiting dynamics of a shrinking interface in a Hele-Shaw cell [J]. *Journal of Fluid Mechanics*, 2021, 910: A41.
[188] Bokman G. T., Supponen O., Makiharju S. A. Cavitation bubble dynamics in a shear-thickening fluid [J]. *Physical Review Fluids*, 2022, 7(2): 023302.
[189] Zhang A. M., Cui P., Wang Y. Experiments on bubble dynamics between a free surface and a rigid wall [J]. *Experiments in Fluids*, 2013, 54: 1602.
[190] Eggers J., Fontelos M. A. Singularities: formation, structure, and propagation [M]. Cambridge, UK: Cambridge University Press, 2015.

[191] Castrejon-Pita J. R., Castrejon-Pita A. A., Thete S. S. et al. Plethora of transitions during breakup of liquid filaments [J]. *Proceedings of the National Academy of Sciences of the United States of America*, 2015, 112(15): 4582-4587.
[192] Maxwell J. C. Statique expérimentale et théorique des liquides soumis aux seules forces moléculaires [J]. *Nature*, 1874, 10(242): 119-121.
[193] Li Y., Sprittles J. E. Capillary breakup of a liquid bridge: Identifying regimes and transitions [J]. *Journal of Fluid Mechanics*, 2016, 797: 29-59.
[194] Dinca V., Patrascioiu A., Fernandez-Pradas J. M. et al. Influence of solution properties in the laser forward transfer of liquids [J]. *Applied Surface Science*, 2012, 258(23): 9379-9384.
[195] Yan J., Huang Y., Xu C. et al. Effects of fluid properties and laser fluence on jet formation during laser direct writing of glycerol solution [J]. *Journal of Applied Physics*, 2012, 112(8): 083105.
[196] Zhang Z., Xiong R., Mei R. et al. Time-resolved imaging study of jetting dynamics during laser printing of viscoelastic alginate solutions [J]. *Langmuir*, 2015, 31(23): 6447-6456.
[197] Turkoz E., Perazzo A., Deike L. et al. Deposition-on-contact regime and the effect of donor-acceptor distance during laser-induced forward transfer of viscoelastic liquids [J]. *Optical Materials Express*, 2019, 9(7): 2738-2747.
[198] Theodorakos I., Kalaitzis A., Makrygianni M. et al. Laser-induced forward transfer of high viscous, non-newtonian silver nanoparticle inks: jet dynamics and temporal evolution of the printed droplet study [J]. *Advanced Engineering Materials*, 2019, 21(10): 1900605.
[199] Turkoz E., Kang S., Deike L. et al. Subthreshold laser jetting via flow-focusing in laser-induced forward transfer [J]. *Physical Review Fluids*, 2018, 3(8): 082201(R).
[200] Mahravan E., Kim D. Bubble collapse and jet formation inside a liquid film [J]. *Physics of Fluids*, 2021, 33(11): 112102.s
[201] Tagawa Y., Peters I. R. Bubble collapse and jet formation in corner geometries [J]. *Physical Review Fluids*, 2018, 3(8): 081601(R).
[202] Cui J., Chen Z. P., Wang Q. et al. Experimental studies of bubble dynamics inside a corner [J]. *Ultrasonics Sonochemistry*, 2020, 64: 104951.
[203] Wang Q., Mahmud M., Cui J. et al. Numerical investigation of bubble dynamics at a corner [J]. *Physics of Fluids*, 2020, 32(5): 053306.
[204] Molefe L., Peters I. R. Jet direction in bubble collapse within rectangular and triangular channels [J]. *Physical Review E*, 2019, 100(6): 063105.
[205] Zhang S., Zhang A. M., Wang S. P. et al. Dynamic characteristics of large scale spark bubbles close to different boundaries [J]. *Physics of Fluids*, 2017, 29(9): 092107.
[206] Xu P., Li B., Ren Z. et al. Dynamics of a laser-induced buoyant bubble near a vertical rigid boundary [J]. *Physical Review Fluids*, 2023, 8: 083601.
[207] Li H., Huang J., Wu X. et al. Dynamic behaviors of a laser-induced bubble and transition mechanism of collapse patterns in a tube [J]. *AIP Advances*, 2020, 10(3): 035210.
[208] Ni B. Y., Zhang A. M., Wang Q. X. et al. Experimental and numerical study on the growth and collapse of a bubble in a narrow tube [J]. *Acta Mechanica Sinica*, 2012, 28(5): 1248-1260.
[209] Xu P., Liu S., Zuo Z. et al. On the criteria of large cavitation bubbles in a tube during a transient process [J]. *Journal of Fluid Mechanics*, 2021, 913: R6.
[210] Brujan E. A., Zhang A. M., Liu Y. L. et al. Jetting and migration of a laser-induced cavitation bubble in a rectangular channel [J]. *Journal of Fluid Mechanics*, 2022, 948: A6.
[211] Brujan E. A., Takahira H., Ogasawara T. Planar jets in collapsing cavitation bubbles [J]. *Experimental Thermal and Fluid Science*, 2019, 101: 48-61.
[212] Wu J., Deijlen L., Bhatt A. et al. Cavitation dynamics and vortex shedding in the wake of a bluff body [J]. *Journal of Fluid Mechanics*, 2021, 917: A26.
[213] Wang Y., Huang C., Du T. et al. Research on ventilation and supercavitation mechanism of high-speed surface-piercing hydrofoil [J]. *Physics of Fluids*, 2022, 34: 023316.
[214] Zhang A. M., Li S. M., Cui P. et al. A unified theory for bubble dynamics [J]. *Physics of Fluids*, 2023, 35(3): 033323.